MASTER THESIS

Analytical Investigation of the Thyroid Set-Point Theory based on Mathematical Modeling and Stability Analysis

submitted to the

Institute of
Analysis and Scientific Computing
TU Wien

under the supervision of

Assistant Prof. Dr. Andreas Körner

by

Corinna Modiz
Matriculation number: 01630052

Vienna, September 2023

Kurzfassung

Die Schilddrüse bildet zusammen mit dem Hypothalamus und der Hypophyse ein geregeltes System, den HPT Komplex, das durch die gegenseitige Beeinflussung der jeweiligen Hormone reguliert wird. Das dynamische System erhält ein körpereigenes Gleichgewicht aufrecht, den so genannten Set-Point, das bei jedem Menschen individuell ist. Die Bestimmung der richtigen Medikamentendosierung für Personen mit Schilddrüsenerkrankungen erfordert daher mehrere ärztliche Behandlungstermine. Um den Behandlungsprozess zu verkürzen und weitere Informationen über die Systemdynamik zu gewinnen, ist eine validierte theoretische Beschreibung des Set-Points erforderlich. Die mathematische Modellierung des HPT Komplexes ist daher ein wichtiges Forschungsgebiet, das mehr Informationen über die gegenseitige hormonelle Beeinflussung und die Bestimmung des endogenen Gleichgewichts liefert.

In dieser Arbeit werden zwei ausgewählte mathematische Modelle näher analysiert. Darüber hinaus werden zwei theoretische Ansätze zur expliziten Bestimmung des Set-Points auf beide Modelle angewandt. Die beiden Ansätze basieren auf der maximalen Krümmung der Reaktionsfunktion der Hypophyse und dem optimalen Gain-Faktor bei der Darstellung des HPT Komplexes als geschlossenes Feedback-System. Da beide mathematischen Modelle das System in Form von Differentialgleichungen beschreiben, wird eine qualitative Analyse durchgeführt, um den Set-Point mit Gleichgewichtspunkten und dem jeweiligen Stabilitätsverhalten in Beziehung zu setzen. In diesem Zusammenhang kann nachgewiesen werden, dass der Set-Point einem zugehörigen global asymptotisch stabilen Gleichgewichtspunkt entspricht. Im Zuge der Modellkalibrierung werden die in dieser Arbeit gewonnenen theoretischen Erkenntnisse mit den tatsächlichen Hormonverläufen von Patienten auf Basis der im AKH Wien erhobenen Daten verglichen und so das Modell validiert. Die Daten wurden im Zuge der Zusammenarbeit mit der Medizinischen Universität Wien (MUW) für diese Arbeit zur Verfügung gestellt.

Abstract

The hypothalamus together with the pituitary and the thyroid gland forms a controlled system, the HPT complex, which is regulated by the mutual influence of the respective hormones. The system maintains an endogenous equilibrium, the so-called set-point, which is individual for each person. Determining the correct medication dosage for patients with thyroid disorders therefore requires several doctoral appointments. In order to shorten the treatment process and gain further information about the system dynamics, a validated theoretical description of the set-point is required. Therefore, mathematical modeling of the HPT complex is an emerging field of research that provides more information about the mutual hormonal influence and the determination of the endogenous balance.

In this work, two selected mathematical models presented in the literature are analyzed in more detail. In addition, two theoretical approaches for the explicit determination of the set-point coordinates are applied to both models. The two approaches are based on the maximum curvature of the pituitary response function and the optimal gain factor when representing the HPT complex as a closed feedback system. Since both mathematical models describe the system in terms of differential equations, a qualitative analysis is conducted to relate the set-point to equilibrium points and the respective stability behavior. In this context, it can be proven that the set-point corresponds to a respective globally asymptotically stable equilibrium point. In the course of model calibration, the theoretical findings obtained in this work are compared with the actual hormone progression of patients based on data collected at the Vienna General Hospital. The data was provided for this work in the course of a cooperation with the Medical University of Vienna (MUW).

Acknowledgment

First and foremost, I would like to express my gratitude to my supervisor, Assistant Prof. Dr. Andreas Körner, for his guidance during this work and the project in the course of which it was written.
I would like to thank my colleagues I had the opportunity to work with during the project, Clara Horvath and Anna Weiskopf, for the productive discussions and their feedback.
I am very grateful to Associate Prof. M.D. Michael Krebs for his advice in medical questions and the time he contributed to the provision of the data that was fundamental for this work.
Moreover, I would like to acknowledge the support of the Center for Technology and Society (CTS) for the project in the course of which this thesis was written.
Finally, I wish to thank my friends and family for their support and especially my partner for his time and constant encouragement.

Eidesstattliche Erklärung

Ich erkläre an Eides statt, dass ich die vorliegende Diplomarbeit selbstständig und ohne fremde Hilfe verfasst, andere als die angegebenen Quellen und Hilfsmittel nicht benutzt bzw. die wörtlich oder sinngemäß entnommenen Stellen als solche kenntlich gemacht habe.

Wien, September 2023

Corinna Modiz

Contents

1 Introduction

According to [MPGGG14], about 11 percent of the European population suffers from thyroid dysfunction. The thyroid is one of the most important organs that regulates the metabolism including cardiovascular activity, fat burning and energy consumption among others. If this system is defective, the hormonal balance is disturbed resulting in fatigue, depression and weight variations, depending on the type of disease. The majority of people affected by thyroid diseases suffers from hyper- or hypothyroidism, in which too much or too little hormone is produced. Although thyroid diseases can be treated by intake of respective synthetic hormones, the determination of the adequate drug dosage requires several doctoral appointments and endocrine level measurements. In addition, the well-being of patients is not guaranteed, even though they may already be in the healthy range of thyroid hormones while taking the medication. This is due to the individual, patient-specific regulation of the thyroid and the resulting non-standardizable drug therapy.
The thyroid in combination with the pituitary and the hypothalamus forms a controlled system, the HPT complex. The secretion of thyrotropin-releasing hormone (TRH) by the hypothalamus stimulates the pituitary to release thyroid-stimulating hormone (TSH) resulting in an increased production and secretion of thyroid hormones, free triiodothyronine (FT3) and free thyroxine (FT4). This in turn leads to a decrease in TSH and TRH and thus forms a negative feedback loop.

The control of the HPT complex is not yet fully understood, so the definition and further investigation of descriptive mathematical models in this context holds the prospect of gaining more information. Simulating the hormonal course in state space and time domain yields more in-depth explanations about the mutual influence of the respective compartments. It is then possible to draw conclusions as to how the individual's balance is physiologically determined and to which components it is most sensitive. In future research, this information may be useful for the individual determination of the correct drug dosage, with the aim of achieving a patient-specific hormonal equilibrium. This contributes to the reduction of medical appointments and blood measurements and to the increase of the patients' well-being. Thus, this work is concerned with the analysis of mathematical models describing the dynamics of the HPT complex.

Several mathematical models of different complexities can be found in literature. According to [DTPM04], one of the first physiologically plausible pituitary models is based on the Michaelis-Menten-Hill kinetics, that describes an enzymatic reaction based on one equation and provides a framework for many dynamic models in the field of systems biology as presented in [YRFSD14].
Its application in modeling HPT dynamics is justified by the resulting log-linear relationship between input and output signal concentration as established in [Fra13], which corresponds

to the mutual dependencies of TSH and thyroid hormones presented in [SLP+90]. Thus, approaches with the objective to describe the time-dependent dynamics of the HPT complex are often based on the Michaelis-Menten equation, including the models introduced in [PMB14], [Goe21] and [YTH+21]. It is developed further to take the influence of other hormones into account, while many models focus on the description of the time-dependent course of TSH and FT4 according to the underlying physiology as described in chapter 2 of this work.
Models of higher complexities are based on up to 15 differential equations that account not only for the time-dependent course of TSH and FT4, but also for other relevant factors. For example, the models presented in [LLXL94], [MM10] and [ESD08] additionally describe the behavior and contribution of other hormones influential to the HPT complex dynamics, including TRH secreted by the hypothalamus, FT3, bound thyroid hormones and several subsystems like kidneys or the peripheral vascular system that can alter the HPT dynamics. Such complex models often focus on specific thyroid diseases and require the collection and measurement of various patient-specific hormonal values. In common patient datasets, these measurements are rarely available and therefore validation of those models is often not feasible.

This work focuses on the determination and investigation of the patient-specific hormonal balance. Therefore simpler models that explicitly or implicitly include the set-point, or present a framework for its derivation, are selected. The model presented in [Goe21] describes the time-dependent dynamics of TSH and FT4 and is developed based on previous publications, [LG14] and [GLS+14], introducing a mathematical framework to derive the set-point in explicit terms. The other model selected for this work is published in [YTH+21]. This approach also describes the time-dependent course of TSH and FT4 and includes a theoretical description of the set-point as the individual hormonal equilibrium. Thus, the mathematical description of the hormonal equilibrium can be further examined in the context of those two models.
Since the models are based on systems of differential equations, they provide the possibility of theoretically determining the equilibrium points. This addresses the question of the validity of the set-point describing the HPT complex equilibrium. The theory established in this work is contextualized with the actual hormone progression of patients based on data collected at the Vienna General Hospital.

The physiological foundation of the HPT complex is described in detail in chapter 2 including the presentation of the patient data.
In chapter 3, the methodology is presented. It covers the two approaches for the mathematical determination of the set-point and the theoretical foundations of sensitivity analysis and parameter identification.
In chapter 4, both models are introduced and the approaches to determine the set-point are applied to the corresponding model functions and examined for consistency. Additionally, the results of the sensitivity analysis of both models are presented and the model-specific parameter identification approaches are described. The qualitative analysis of systems of differential equations provides information on local and global long-term stability behavior.

In chapter 5, the general equilibrium point of a system of differential equations is thus determined for both models including the stability behavior. Additionally, the derived set-point equations are analyzed in this context.
To contextualize the theoretical analysis with patient data, the calibration results are presented in chapter 6. It includes patient-specific hormonal curves in state space and time domain resulting from parameter identification of different models and calibration approaches for three exemplary patients. The numerical results focusing on the final error are presented for all patients included in the data set.
In conclusion, the following work is concerned with two selected mathematical models of the HPT complex based on set-point derivation, equilibrium behavior and parameter identification.

2 Physiological Foundation

The hypothalamus-pituitary-thyroid complex forms a regulated system through the mutual influence by secretion of the associated hormones. This system forms the basis for a simulation of the thyroid hormone regulation and is therefore described with reference to physiological processes and associated diseases in this chapter. Since the simulation is based on fitting mathematical models to measurements, the patient data is also presented in this chapter. This includes the selection process of relevant patients, details of medical history and statistical parameters.

2.1 The Hypothalamus-Pituitary-Thyroid Complex

According to [Des91] and [Hic95], the thyroid is a butterfly shaped endocrine organ and is located in front of the thyroid cartilage of the larynx. It consists of two lobes connected by a bridge, the isthmus. The thyroid gland has a variety of effects, but mainly influences the stimulation of the basal metabolic rate with the help of the hormones secreted. This includes energy consumption, fat burning, heat production and cardiovascular activity.
The production and secretion of thyroid hormones is controlled by the hypothalamus and the pituitary. Therefore, this control circuit is referred to in the following as the hypothalamus-pituitary-thyroid (HPT) complex which is schematically illustrated in Fig. 2.1.

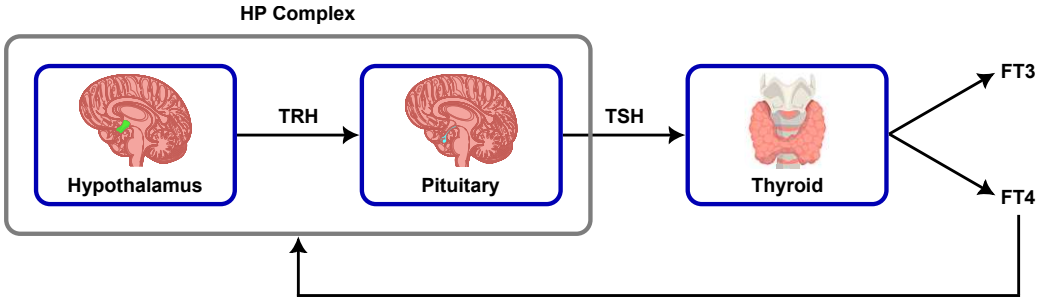

Figure 2.1: Block diagram of a general closed-loop HPT feedback system including two blocks.

The main control hormone of the thyroid is the pituitary hormone thyrotropin (TSH), whose synthesis and release is influenced by thyrotropin-releasing hormone (TRH) from the hypothalamus. An increase in the concentration of TSH has various effects on the thyroid. It stimulates the iodine uptake in thyroid epithelial cells, which is an important part of the final thyroid hormones. Additionally, it increases the synthesis and release of the thyroid hormones, thyroxine (T4) and triiodothyronine (T3), and the formation of their preliminary

stage, thyreoglobulin. Thyroid hormones, in turn, lead to a decreased number of TRH receptors on the pituitary gland, which reduces TSH and subsequently T3 and T4 secretion. Therefore, the HPT complex includes a negative feedback loop. The serum concentration of TRH is very low and, according to [Pas19], the TRH secretion is only affected to a small extend by the negative feedback of thyroid hormones. Since additionally the systemic contribution of the two compartments is similar, the hypothalamus and pituitary gland are combined into the HP complex when modeling their hormone regulation.
The formation and storage of T3 and T4 takes place in the thyroid and follicular cells. Iodine is absorbed into the thyroid cell and after oxidation is incorporated into the thyreoglobulin. The compound is then transported to the follicular cells of the thyroid gland and stored there. Upon release, it returns to the thyroid cell where the carrier molecule thyroglobulin is split off and free T3 (FT3) and free T4 (FT4) are secreted into the blood. Only the free thyroid hormone can exert an effect. Most of the T3 hormone does not originate directly from the thyroid, but is created during mono-deiodisation, the detachment of an iodine atom, of T4. Therefore, the simulation of the HPT complex is mostly restricted to the effective, most abundant hormone in the blood, FT4.
When the thyroid hormone balance is in equilibrium and the thyroid is in a healthy condition, it is called a state of euthyroidism. This state is indicated by hormonal concentrations of TSH and FT4, specified as [TSH] and [FT4], in the normal range. The corresponding intervals according to [Pan11] are listed in Table 2.1. The units of [TSH] and [FT4] are not always consistent in the literature, but can be convertedto allow a comparison of different modling approaches, see chapter 4. The conversion factor of $\mathrm{pg} \cdot \mathrm{mL}^{-1}$ to $\mathrm{pmol} \cdot \mathrm{L}^{-1}$ for [FT4] is 1.2872.

Parameter	Unit	Normal Range
TSH	$\mathrm{mU} \cdot \mathrm{L}^{-1}$	$[2.5, 4]$
FT4	$\mathrm{pg} \cdot \mathrm{mL}^{-1}$	$[7, 18]$

Table 2.1: Normal ranges of TSH and FT4.

If the amount of thyroid hormone produced is higher or lower than the normal range, this is called hyper- or hypothyroidism, which are explained in detail in section 2.2.

2.2 Thyroid Gland Diseases

When the thyroid hormone system described in the previous section is in balance, it is called euthyroidism. If too little or too much thyroid hormone is produced, the condition is referred to as hypothyroidism or hyperthyroidism, respectively. Since the aim of this work is the simulation of the hormonal course of patients suffering from hypothyroidism, this section focuses on a short introduction of its etiology, disease pattern and treatment based on [BBG+21]. Some of the patients whose simulation results are presented in chapter 6 were prescribed a drug dose for hyperthyroidism, so a brief description of this condition is provided.
Hypothyroidism occurs when there is a deficiency of thyroid hormone or insufficient action of thyroid hormone. Hypothyroidism is most commonly caused by autoimmune destruction

of thyroid tissue, Hashimoto's thyroiditis. Corresponding laboratory testing often identifies antibodies directed against thyreoglobulin, among others. Rarely, other causes of thyroid destruction, e.g. tumors, are present. In Hashimoto's thyroiditis, transient hyperthyroidism may occur initially. Generally, these disorders are also called primary hypothyroidism. In addition, secondary hypothyroidism may occur in the absence of pituitary TSH. The most common symptoms of hypothyroidism are weight gain, hair loss, decrease in concentration and sensation of cold. The most important diagnostic criterion for the assessment of thyroid function is the determination of TSH. In primary hypothyroidism, TSH is elevated and FT4 is decreased in the presence of undisturbed pituitary function. Only in pituitary secondary hypothyroidism are both TSH and FT4 reduced. The therapy of manifest hypothyroidism consists in the substitution of thyroxine. The substitution is started gradually, then the dose is increased until euthyroid function is achieved. Usually, according to [BBG+21], doses of about 1.5 µg per kilogram body weight are administered.
Hyperthyroidism describes the presence of too much thyroid hormone. The most common cause of this disease are various adenomas or an autoimmune disease due to antibodies against TSH receptors, also known as Graves' disease. Primary hyperthyroidism is the most common form, secondary hyperthyroidism with causes in the pituitary gland is extremely rare. Typically found are cardiac arrhythmias, elevated body temperature, muscle weakness, restlessness, sleep disturbance and weight loss. The most important diagnostic criterion for the assessment of hyperthyroidism is also the determination of TSH, supplemented by the peripheral thyroid hormone values. In hyperthyroidism, TSH is decreased and peripheral thyroid hormone levels are increased. Therapy of manifested hyperthyroidism is usually only temporary thyrostatic drug therapy, long-term therapy consists of therapy of the underlying disease. According to [BBG+21], for short-term thyrostatic therapy, thiamazole with an initial dose of 15-40 mg per day is most commonly used.

2.3 Data collected in a Clinical Study

To build an understanding about the underlying physiological processes and to calibrate and verify the mathematical models presented in chapter 4, a retrospective study at Vienna General Hospital, conducted by the Medical University of Vienna (MUW), was performed. In accordance with the ethics agreement, the data was made available anonymously for scientific use. Initially, 71 patients were included and data such as date of medical consultation, age, diagnosis, current medication, TSH concentration in µIU/mL and FT4 concentration in ng/dL along with other medical parameters was collected. All patients involved in the study suffer from different types of hypothyroidism and hyperthyroidism. The following work aims to gather more information about the mutual influence of thyroid hormones, especially in the context of hypothyroidism, so patients that do not meet these criteria are excluded from the data set. After a subsequent removal of those patients with missing data points, a data base consisting of 25 patients in total remains.
Figure 2.2 shows the data points of all patients of the data set with respect to TSH and FT4. The majority of the points can be found in the normal range for both TSH and FT4, indicated by the dotted gray lines. The figure also indicates that the data points follow the log-linear relationship of TSH and FT4 presented in [SLP+90].

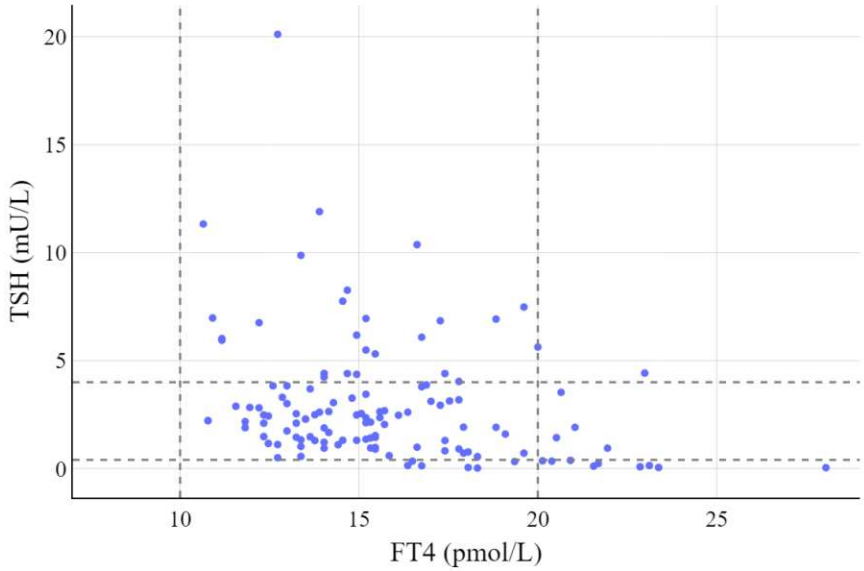

Figure 2.2: Data points of both TSH and FT4 of the base data set consisting of 25 patients. The normal range is indicated by the dashed gray lines.

Additionally, the physiological dynamics discussed in detail in section 2.1 can be observed in Fig. 2.2. If the TSH value of one data pair is high, the respective FT4 value can be found in the lower range and vice versa. For example, the maximum FT4 value of 28.05 pmol/L corresponds to the minimum TSH value of 0.02 mU/L.

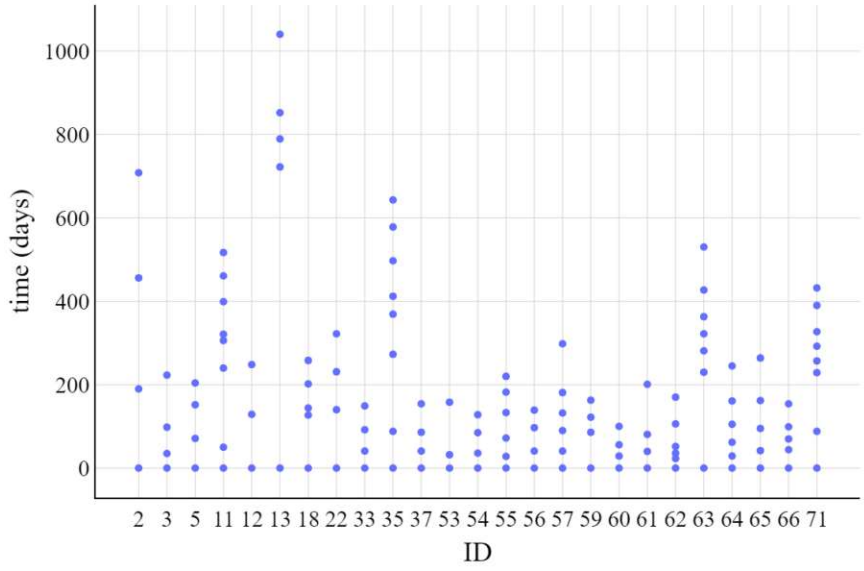

Figure 2.3: Time of the measurements in days for the individual patients..

All patients included in the data set have a different time and number of medical appointments. Additionally, the measurement dates also vary in the time interval between measurements, as shown in Fig. 2.3. The maximum time period for which data is available can be found for patient 13. The time between the first and last data point is almost 2.85 years. The minimum range between the first and the last measurement is 100 days and can be found with patient 60.

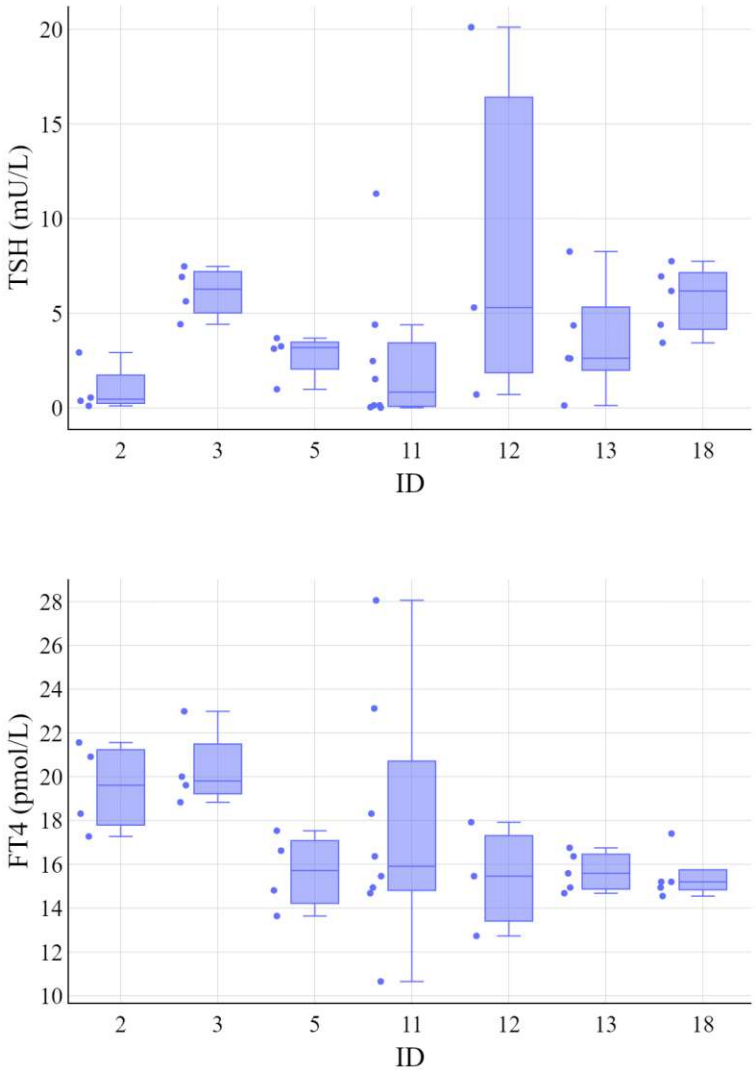

Figure 2.4: Distribution of the measurement points of both hormones of seven exemplary patients.

Figure 2.4 shows the exemplary distributions of TSH and FT4 measurements of seven patients. The number of measurements per patient ranges from a minimum of three to a maximum of nine.

A maximum TSH value of 20.11 mU/L of the entire data set is found for patient 12, while the minimum of 0.02 mU/L was measured with patient 11. This patient also shows the maximum and minimum FT4 value of 28.05 and 10.65 pmol/L. While patient 12 has the widest range of TSH, patient 11 has the widest range of FT4, as shown in Fig. 2.4.
The presented data and underlying physiology of the HPT complex can be used to calibrate and verify the models introduced in chapter 4 based on the methodology described in detail in the following chapter.

3 Mathematical Modeling and Framework

Modeling and simulation is an important and broadly applied tool to further investigate correlations, gain insight and make predictions of a system. There are several definitions of the phrase modeling and simulation. According to [BA19], modeling refers to the creation of an object, that is, a model, which is subsequently used for experimentation. A model is defined as a representation or abstraction of a system, and the corresponding experimentation corresponds to the term simulation. With the help of such models, complex systems can be limited to the crucial components to enable a more detailed interpretation.
The Hypothalamus-Pituitary-Thyroid (HPT) complex described in chapter 2.1 strongly depends on by the mutual influence of its components and contains an individual hormonal equilibrium. This equilibrium can be mathematically derived and further investigated by introducing the maximum curvature theory. Additionally, it can be defined by representing the complex as a feedback system, which additionally provides the possibility to gain further information about the physiological behavior. To validate those approaches in correspondence with the respective mathematical models, that are introduced in chapter 4, the procedure pursued for parameter identification. Those three methods including the theoretical background are introduced in this chapter.

3.1 Maximum Curvature Theory and Homeostatic Set-Point

According to [LG14], a system described by a negative feedback loop contains a reference point, or set-point, in normal operation. As described in detail in chapter 2.1, the HPT complex can be represented as a system consisting of two compartments whose mutual influence is represented by a negative feedback loop. In this system, the HP complex acts as a controller for the thyroid gland, regulating the production of hormones into a very small range of healthy or euthyroid equilibrium. This framework leads to the following physiological definition of the set-point.

Definition 1. *The set-point of an intact HPT axis of a healthy euthyroid person represents the ideal personalized thyroid function target that results in an optimal healthy state. [LG14]*

Even the slightest deviation from this point, e.g. due to physiological variations, is registered by the HP complex. In response, the hormones are regulated back into the original state of equilibrium.
Several approaches on the mathematical derivation of the set-point are introduced for a specific model of the HPT complex in [LG14] and discussed in detail in 4.1. One of those approaches is the computation of the point of maximum curvature of the function describing the response of the HP complex on a specific FT4 concentration, represented as [FT4]. This approach is based on the authors of the source publication [LG14] finding that the knee

region of the response function is always in the normal range for both hormones. This resulted in localizing the set-point at the knee region. The set-point is the point around which the pituitary is most sensitive to any changes in concentration of [FT4]. Therefore, the set-point is ultimately defined as the point of maximum curvature, which corresponds to the point of maximum sensitivity.

Definition 2. *The curvature K_g of a function $g : \mathbb{R} \to \mathbb{R}, a \mapsto g(a)$ is defined as*

$$K_g = \frac{\frac{\mathrm{d}^2 g}{\mathrm{d}a^2}}{\left(1 + \left(\frac{\mathrm{d}g}{\mathrm{d}a}\right)^2\right)^{\frac{3}{2}}}. \tag{3.1}$$

Based on this definition, an explicit representation for the set-point can be given.

Definition 3. *The set-point of the HPT complex is specified as the unique point of the response function of the pituitary, $f([\mathrm{FT4}]) = [\mathrm{TSH}]$, that fulfills*

$$\frac{\mathrm{d}K_f}{\mathrm{d}[\mathrm{FT4}]} = 0. \tag{3.2}$$

The established maximum curvature theory introduces the first approach to theoretically determine the set-point and will be applied to selected mathematical models in the following work. The theoretical basis for the second definition of the set-point is presented in the following section.

3.2 Feedback Systems and Gain Factor Analysis

To analyze the HPT behavior from a control engineering perspective, the HPT system described in section 2.1 is represented as a feedback control system. This approach including the preceding theoretical part is described in more details in this section.
As described in detail in [AM08], control systems can be represented by block diagrams in combination with transfer functions.

Definition 4. *Transfer functions describe the mapping of the input u of a control system, shown in Fig. 3.1, to the output v and is defined as*

$$G(s) = \frac{v(s)}{u(s)}. \tag{3.3}$$

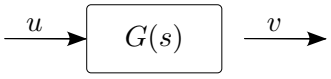

Figure 3.1: Block diagram with input and output signal.

In a system consisting of several blocks, transfer functions can be defined to link different signals by considering the transfer functions of the respective subsystems and applying the corresponding arithmetic rules. These principles determine the transfer function depending

on the way the blocks are interconnected, where transfer functions of two blocks connected in series are multiplied, those connected in parallel are summed.
In a control system consisting of different dynamic subsystems, feedback is defined by interconnected subsystems, that influence each other and thus show strongly coupled dynamics. A representation of a closed-loop feedback system is shown in Fig. 3.2.

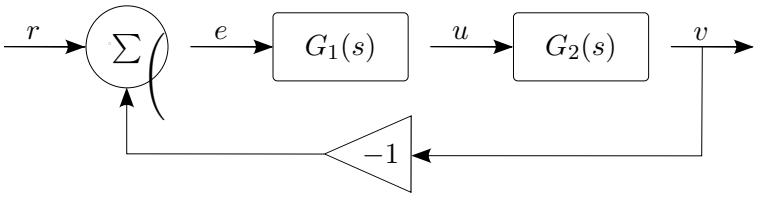

Figure 3.2: Block diagram of a closed-loop feedback system including two blocks.

The output signal v is compared against the reference signal r that determines the target value of the control system. The overall transfer function $G(s)$ of the system shown in Fig. 3.2 can be expressed explicitly using the formulas for serially connected blocks in combination with (3.3). It follows that

$$e(s) = v(s) - r(s), \quad u(s) = G_1(s)e(s), \quad v(s) = G_2(s)u(s),$$
$$\Rightarrow v(s) = \underbrace{\frac{G_1(s)G_2(s)}{1 + G_1(s)G_2(s)}}_{=G(s)} r(s). \tag{3.4}$$

The transfer function of a control system has many important properties that provide insights into the systems behavior, one of those is the so-called zero frequency gain or gain factor describing the transfer function of a steady-state system.

Definition 5. *The zero frequency gain G is defined as the corresponding transfer function $G(s)$ at $s = 0$ and represents the ratio of the steady-state value of the output to a step input. [AM08]*

The loop transfer function $G_L(s)$ was introduced by Nyquist to identify constraints on the occurrence of oscillations in a feedback loop.

Definition 6. *The loop transfer function $G_L(s)$ of a feedback system is defined as the transfer function obtained by breaking the feedback loop. [AM08]*

As a result, the loop transfer function of the system shown in Fig. 3.2 is given as

$$G_L(s) = G_1(s)G_2(s). \tag{3.5}$$

The Hypothalamus-Pituitary-Thyroid complex described in section 2.1 can be represented as a closed-loop feedback system as shown in Fig. 3.3 and established in more detail in [GLS+14]. This statement is based on a small signal representation of the HPT complex around the set-point and the assumption that the characteristics of the HP complex and the thyroid are continuous and differentiable and therefore fulfill the conditions for linearization in the region of interest.

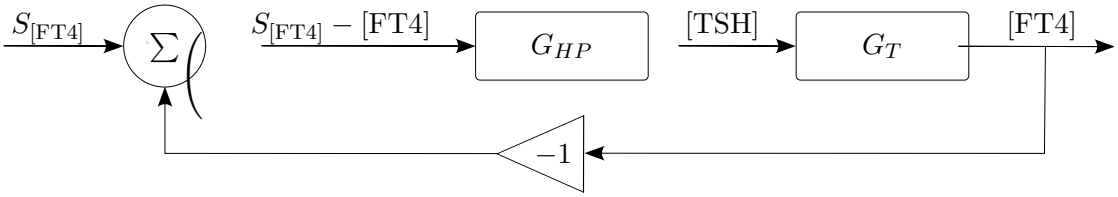

Figure 3.3: HPT complex represented as negative feedback closed-loop system.

The HP complex controls the thyroid by the secretion of [TSH] which depends on the input signal $S_{[FT4]} - [FT4]$. The input signal consists of the intrinsic physiological set-point $S_{[FT4]}$ as defined in section 3.1 and the feedback signal [FT4]. The thyroid complex secretes an amount of [FT4] in direct proportion to the input or control signal [TSH].
Following the definitions 5 and 6 and [GLS+14], the loop gain of the HPT complex can be defined as $G_L = |G_{HP}G_T|$. In line with definition 3.3, both G_{HP} and G_T describe the gain factor as a ratio between the input and output signal. According to [GLS+14], when referring to the HPT complex, the interpretation refers to the measure of the variation of the output signal to a corresponding relatively small variation of the input signal. It follows that

$$\mathrm{d}[\mathrm{FT4}]G_{HP} = \mathrm{d}[\mathrm{TSH}], \quad \mathrm{d}[\mathrm{TSH}]G_T = \mathrm{d}[\mathrm{FT4}]. \tag{3.6}$$

Analogous to the description of the general feedback system shown in Fig. 3.2, the ratio between input and output signal is given as

$$[\mathrm{FT4}] = \frac{G_L}{1 + G_L} S_{[\mathrm{FT4}]}. \tag{3.7}$$

This equation describes the expected behavior since the fraction tends to 1 for very large values of G_L. The amount of [FT4] is therefore kept close to the intrinsic set-point value. If G_L is smaller than unity, [FT4] will decrease against S_{FT4} resulting in a loss of interaction between thyroid and HP complex and therefore an open loop system.
Using the determined loop gain, points of extrema can be investigated. In line with the definitions given in section 3.1, the HPT complex operates at its optimum when the amount of [FT4] and [TSH] correspond to the target set-point. Thus it can be derived by computing the extremum according to the following definition.

Definition 7. *The set-point of the HPT complex represented as negative feedback closed-loop system as in Fig. 3.3 is defined as the point where the loop gain $G_L = G_T G_{HP}$ operates at its optimum. Under the condition that G_L depends only on one hormone concentration, it can be derived by setting the corresponding derivative to zero. [GLS+14]*

According to this definition, the gain factor analysis provides the possibility to derive an explicit expression of the set-point. Combined with the maximum curvature theory, it can be applied to selected mathematical models to gain further information about the individual set-point coordinates.

3.3 Sensitivity Analysis

In general, sensitivity analysis is used to determine the behavior of specific dependent variables of a model in response to changing independent variables. According to [NEB11], sensitivity analysis is crucial for the determination of use and meaning of model parameters and thus is an important prerequisite in model identification and calibration. A quantitative sensitivity analysis based on the variance-based Sobol' method [Sob01] described in detail in [Sal02] is conducted for the mathematical models introduced in chapter 4. In the course of this analysis, Sobol' sensitivity indices of various orders are computed, explaining the proportion of variance that each dependent model parameter, or their interaction, has in the unconditional variance of the model output.
In the course of the sensitivity analysis chosen for this work, the most important factor, which is defined as the factor resulting in the greatest reduction of in the variance V of the model output Y, can be determined. As presented in detail in [Sal02], the theoretical derivation of the Sobol' indices is based on the mathematical model

$$Y = g(X) = g(X_1, X_2, \ldots, X_n), \tag{3.8}$$

where Y denotes the model output and some of the input variables X_i, with $i \in 1, 2, \ldots, n$, are uncertain. Additionally, the parameters X_i are assumed to be independent and identically distributed. The Sobol' decomposition of the model function (3.8), published in [Sob93] and explained in detail in [TCC20], is defined as

$$g(X) = g_0 + \sum_{i=1}^{n} g_i(X_i) + \sum_{i=1}^{n} \sum_{j>i}^{n} g_{ij}(X_i, X_j)) + \ldots + g_{12\ldots n}(X_1, X_2, \ldots, X_n), \tag{3.9}$$

using the conditional expectation E and

$$g_0 = E(Y), \tag{3.10}$$
$$g_i(X_i) = E(Y|X_i) - g_0, \tag{3.11}$$
$$g_{ij}(X_i, X_j) = E(Y|X_i, X_j) - g_i - g_j - g_0, \ldots. \tag{3.12}$$

Based on this definition, the general decomposition scheme established in [Sob93] can be applied to the total variance of the output $V(Y)$ resulting in

$$V(Y) = \sum_{l} V(g_l(X_l)) \quad \text{with} \quad l \subseteq \{1, ..., n\} \quad \text{and} \quad l \neq \emptyset, \tag{3.13}$$

where $V(g_l(X_l))$ denotes the conditional variance of the conditional expectation depending on the subset l. Thus, the Sobol' index associated to the subset l is defined as the ratio between the contribution given by the interaction among the components of l for the model variance and the total variance itself [TCC20], i.e.

$$S_l = \frac{V(g_l(X_l))}{V(Y)}. \tag{3.14}$$

The Sobol' indices of first order are given as

$$S_i = \frac{V(g_i(X_i))}{V(Y)}, \quad i = 1, \ldots, n, \tag{3.15}$$

and describe the contribution of the variance of one parameter to the total model variance. The effect of the interaction between two parameters, that is not described by the indices of first order, is determined by the Sobol' index of second order,

$$S_{ij} = \frac{V(g_{ij}(X_{i,j}))}{V(Y)}, \quad 1 \leq i < j \leq n. \tag{3.16}$$

The impact on the model output variance of a specific parameter including all its interactions is described by the total Sobol' index $S_{12\ldots n}$.
For the sensitivity analysis of the models presented in chapter 4, the python library SAlib was used. Since the main focus of this work is the set-point and the equilibrium point of the models, respectively, the analysis was limited to the last point in time of the time-dependent solution curve of the differential equation system. The analysis can be extended to include more time points distributed over the entire time course, which requires higher computational costs.

3.4 Parameter Identification

Parameter identification describes the determination of an optimal parameter set which obtains the best fit of a model to experimental data. The problem can be formulated with respect to the time domain in line with [CS15] as follows.
The model is defined by $\tilde{z}(t,\theta) = (\tilde{z}_1(t,\theta), ..., \tilde{z}_d(t,\theta)) \in \mathbb{R}^d$ fulfilling $\frac{\mathrm{d}}{\mathrm{dt}}\tilde{z} = f(\tilde{z},\theta)$ with $\tilde{z}(t_0,\theta) = \tilde{z}_0$. The vector $\theta = (\theta_1, ..., \theta_q) \in \mathbb{R}^q$ contains the model parameters. Let $z_{k,l}$ denote the experimental data with $k = 1, ..., d$ corresponding to the k-th component of $\tilde{z}$ and $l = 1, ..., n$ describing the l-th point in time. Thus, the corresponding model evaluation would be $\tilde{z}_k(t_l,\theta)$.
The objective is thus to fit the model to the data by estimating parameters in the course of minimizing the error function $\xi(\theta)$. The selection of this objective function is essential as it determines the fit of the calibration. Here and in the following, it is defined as the sum of the respective normalized mean squared errors of z_k following

$$\xi(\theta) = \frac{1}{n}\sum_{k=1}^{d}\sum_{l=1}^{n}\frac{(\tilde{z}_k(t_l,\theta) - z_{k,l})^2}{(z_{k,l}^{\max} - z_{k,l}^{\min})}. \tag{3.17}$$

The final objective of the calibration is the minimization of ξ with respect to θ.
There are several algorithms that serve the purpose of minimizing an objective function by varying the model parameters. These include the differential evolution algorithm presented in [SP97] and used for data-based model analysis in chapter 6. The approach represents a global optimization algorithm which converges faster, is robust and requires few control variables. The method is not gradient-based and therefore does not require the objective function to be differentiable. Differential evolution is designed as a stochastic direct search method based on parameter vector populations.

The process is briefly concluded in the following paragraph, but is described in detail in [SP97]. The initial population consisting of N parameter vectors is chosen randomly for each generation G. New vectors are then defined by manipulating and combining three already existing vectors in the course of a process called mutation. This operation is followed by the so-called selection where the new and old parameter vectors are compared with respect to the corresponding value of the cost function. Depending on the results of this competition, one of them is selected as part of the next mutation. Each vector of each generation is compared once following this approach.
The hyper parameters of the differential evolution algorithm used for the calibration were determined according to the default parameters of the pythons implementation summarized in Table 3.1.

Parameter	Value
maxiter	1000
popsize	15
tol	0.01

Table 3.1: Hyper parameters of applied differential evolution algorithm.

The parameter maxiter determines the maximum number of generations and popsize influences the total population size. According to [CTZFG+21], the optimal population size for a problem of lower dimension is larger than 50. Concerning this problem, this is not realizable due to the large computation time. The relative tolerance for convergence is determined by the parameter tol.

4 Mathematical Models including a Homeostatic Set-Point

The mutual influence of thyroid hormones can be described by mathematical models that approximate their course in the state space and their long-term behavior. Modeling the thyroid complex by differential equations furthermore offers the possibility to investigate the physiological hormonal equilibrium by analyzing the mathematical equilibrium of the differential equations. Two mathematical models considered in this work include a set-point - either explicitly or implicitly. The model introduced in [Goe21] presents an exponential correlation between both TSH and FT4 and includes theories for the mathematical derivation of the set-point. The system of differential equations presented in [YTH+21] is chosen as comparative model to apply the set-point computation and analysis on the set-point explicitly described in the model.

4.1 A Minimal Model of the Hypothalamus-Pituitary-Thyroid Axis

The system of differential equations presented in [Goe21] represents the behavior of [TSH], the concentration of TSH, over time in negative exponential dependence on [FT4], the concentration of FT4, and vice versa, according to

$$\begin{aligned} \frac{\mathrm{d}[\mathrm{TSH}]}{\mathrm{d}t} &= \frac{S}{\exp(\varphi\,[\mathrm{FT4}])} - [\mathrm{TSH}]\,, \\ \frac{\mathrm{d}[\mathrm{FT4}]}{\mathrm{d}t} &= A - \frac{A}{\exp(\alpha\,[\mathrm{TSH}])} - [\mathrm{FT4}]\,. \end{aligned} \tag{4.1}$$

The model includes four parameters $S, \varphi, A, \alpha \in \mathbb{R}^+$, where φ and α represent the decay rate of [TSH] and [FT4], respectively.
In [LG14], a mathematical framework is established to analytically derive the individual euthyroid state which corresponds to the set-point based on the maximum curvature theory and gain factor analysis, which are explained in detail in section 3.1 and 3.2. Those two theories result in explicit mathematical terms for the set-point coordinates of both hormones and will be presented, analyzed and combined in the following sections. Their definition, however, makes it possible to evaluate its applicability to other models, such as the unified model, which will be presented later in this work.
Both approaches are based on the equilibrium state of system (4.1), which is described by

$$\frac{\mathrm{d}[\mathrm{TSH}]}{\mathrm{d}t} = 0, \quad \frac{\mathrm{d}[\mathrm{FT4}]}{\mathrm{d}t} = 0. \tag{4.2}$$

Transforming the equations (4.1) results in

$$[\mathrm{TSH}] = \frac{S}{\exp(\varphi\,[\mathrm{FT4}])}, \tag{4.3}$$

$$[\mathrm{FT4}] = A - \frac{A}{\exp(\alpha\,[\mathrm{TSH}])}. \tag{4.4}$$

In the further work, the functions (4.3) and (4.4) will be referred to as HP-function and T-function, respectively.
Further establishment on the maximum curvature theory, the gain factor analysis and the respective combination provides the possibility to reduce the number of parameters by deriving a dependency on the set-point coordinates of [TSH] and [FT4]. This approach will also be presented and analyzed in the following sections.
In the following sections, ([FT4] , [TSH]) will be referred to as (x, y) for readability purposes.

4.1.1 Application of the Maximum Curvature Theory to the Hypothalamus-Pituitary Function

Following the framework presented in [LG14], the maximum curvature theory, that is described in detail in section 3.1, is applied to the HP-function. Therefore, the curvature (3.1) of the HP-function (4.3) is calculated, resulting in

$$K_y = \frac{S\varphi^2 \exp(-\varphi x)}{\left(1 - S^2\varphi^2 \exp(-2S\varphi x)\right)^{\frac{3}{2}}}. \tag{4.5}$$

The maximum of K_y is determined using the derivative $\frac{\mathrm{d}K_y}{\mathrm{d}x}$ and quotient rule resulting in

$$\begin{aligned}
\frac{\mathrm{d}K_y}{\mathrm{d}x} &= \frac{\left(S\varphi^3 \exp(-\varphi x)\right)\left(2S^2\varphi^2 \exp(-2\varphi x) - 1\right)}{\left(1 + S^2\varphi^2 \exp(-2\varphi x)\right)^{\frac{5}{2}}} = 0 \\
&\Leftrightarrow \left(S\varphi^3 \exp(-\varphi x)\right)\left(2S^2\varphi^2 \exp(-2\varphi x) - 1\right) = 0 \\
&\Leftrightarrow 2S^2\varphi^2 \exp(-2\varphi x) - 1 = 0 \\
&\Leftrightarrow x_{sp} = \frac{\ln(\sqrt{2}S\varphi)}{\varphi}.
\end{aligned} \tag{4.6}$$

Substituting (4.6) in (4.3) results in

$$y_{sp} = \frac{1}{\sqrt{2}\varphi}. \tag{4.7}$$

The maximum curvature theory applied to the HP-function is exemplary illustrated in Fig. 4.1. It can be observed that the analytically derived set-point $(x_{sp}^{\mathrm{mch}}, y_{sp}^{\mathrm{mch}})$ can be found at the point where the curvature of the HP-function reaches its maximum. In addition, the first and second derivatives of the curvature are plotted to verify the condition that the second derivative is less than zero at the point of maximum curvature.

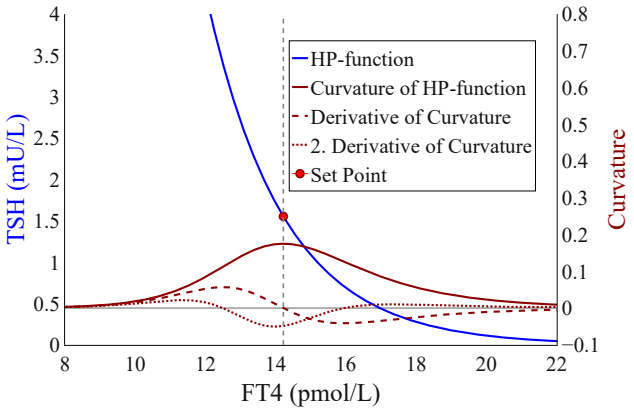

Figure 4.1: HP-function and set-point computed based on the corresponding curvature function.

4.1.2 Application of the Maximum Curvature Theory to the Thyroid Function

The maximum curvature theory states that the set-point is the point of highest sensitivity of a function to input-variations. Therefore, the maximum curvature theory should also be applicable to (4.4) while not contradicting the previous results. Following the same framework of determining the point of maximum curvature implies

$$K_x = \frac{-A\alpha^2 \exp(-\alpha y)}{(1 + A^2\alpha^2 \exp(-2\alpha y))^{\frac{3}{2}}}, \tag{4.8}$$

and

$$\begin{aligned}\frac{\mathrm{d}K_x}{\mathrm{d}y} &= \frac{\left(1 + A^2\alpha^2 \exp(-2\alpha y)\right)^{\frac{1}{2}}\left(A\alpha^3 \exp(-\alpha y) + A^3\alpha^5 \exp(-3\alpha y) - 3A^3\alpha^5 \exp(-3\alpha y)\right)}{\left(1 + A^2\alpha^2 \exp(-2\alpha y)\right)^{\frac{1}{2}}} \\ &= \frac{A\alpha^3 \exp(-\alpha y)\left(1 - 2A^2\alpha^2 \exp(-2\alpha y)\right)}{\left(1 + A^2\alpha^2 \exp(-2\alpha y)\right)^{\frac{5}{2}}}\end{aligned} \tag{4.9}$$

The point of maximum curvature is determined following

$$\begin{aligned}\frac{\mathrm{d}K_x}{\mathrm{d}y} = 0 &\Leftrightarrow A\alpha^3 \exp(-\alpha y)\left(1 - 2A^2\alpha^2 \exp(-2\alpha y)\right) = 0 \\ &\Leftrightarrow 1 - 2A^2\alpha^2 \exp(-2\alpha y) = 0 \\ &\Leftrightarrow y_{sp} = \frac{\ln(\sqrt{2}A\alpha)}{\alpha}.\end{aligned} \tag{4.10}$$

Substituting y in (4.4) results in

$$x_{sp} = A - \frac{1}{\sqrt{2}\alpha}. \tag{4.11}$$

Therefore, this approach also results in an explicit representation of x_{sp}^{mct} and y_{sp}^{mct} referring to the set-point of [FT4] and [TSH], respectively. The approach including all respective functions and the set-point is shown in Fig. 4.2. This plot also shows that the second derivative fulfills the requirement to be unequal to zero at the point of maximum curvature.

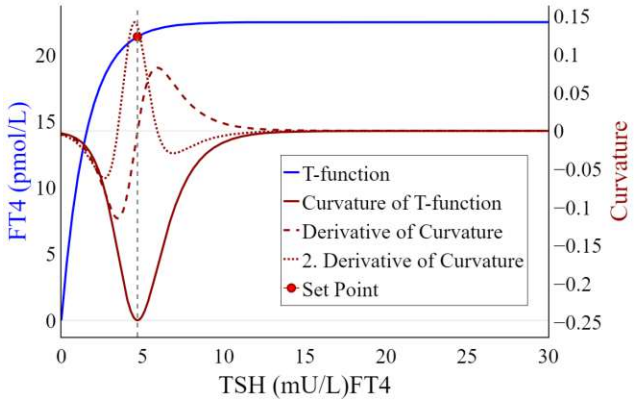

Figure 4.2: T-function and set-point computed based on the corresponding curvature function.

4.1.3 Gain Factor Analysis

The set-point can also be determined by analyzing the optimal overall gain factor G while referring to the system of differential equations (4.1) as a closed-loop system as shown in Fig. 4.3.

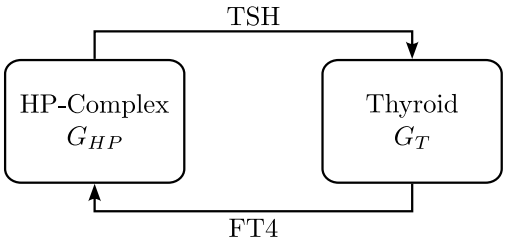

Figure 4.3: HPT model illustrated as closed-loop system.

In general, the gain $G = \frac{\mathrm{d}v_{out}}{\mathrm{d}v_{in}}$ is determined by finding the quotient of the output signal v_{out} to the input v_{in} as established in 3.2. It follows that the gain for the HP-Complex, G_{HP}, is described by

$$G_{HP} = \frac{\mathrm{d}y}{\mathrm{d}x} = \frac{\mathrm{d}}{\mathrm{d}x} S\exp(-\varphi x) = -S\varphi\exp(-\varphi x) \overset{(4.3)}{=} -\varphi y, \tag{4.12}$$

using a substitution of (4.3) in (4.12). The same framework can be applied to determine

the gain for the Thyroid-Complex, G_T, following

$$G_T = \frac{\mathrm{d}x}{\mathrm{d}y} = \frac{\mathrm{d}}{\mathrm{d}y}\left(A\left(1-\exp(-\alpha y)\right) = \alpha A \exp(-\alpha y)\right). \tag{4.13}$$

By serially combining the two compartments, the overall gain can be determined by

$$G(x,y) = |G_{HP}G_T| = A\alpha\varphi y \exp(-\alpha y). \tag{4.14}$$

The overall gain only depends on y and thus $G(x,y) = G(y)$. Therefore, the optimal value of G is determined using only the derivative with respect to y, which leads to

$$\begin{aligned}\frac{\mathrm{d}G}{\mathrm{d}y} = 0 &\Leftrightarrow \frac{\mathrm{d}}{\mathrm{d}y} A\alpha\varphi y \exp(-\alpha y) = 0\\ &\Leftrightarrow A\alpha\varphi \exp(-\alpha y) - A\alpha^2\varphi y \exp(-\alpha y) = 0\\ &\Leftrightarrow A\alpha\varphi \exp(-\alpha y)\left(1-\alpha y\right) = 0\\ &\Leftrightarrow y = \frac{1}{\alpha}.\end{aligned} \tag{4.15}$$

Substituting (4.15) into (4.4) results in

$$x = A\left(1-\exp(-1)\right). \tag{4.16}$$

Both theories result in an explicit representation for x_{sp}^{gf} and y_{sp}^{gf} referring to the set-point of [FT4] and [TSH], respectively. The approach is represented in Fig. 4.4 with exemplary parameters.

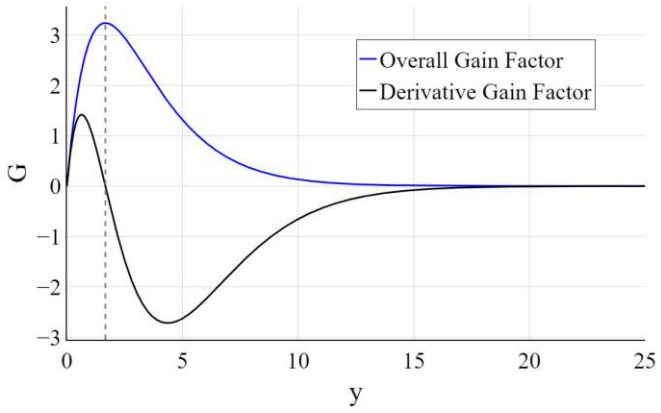

Figure 4.4: Exemplary representation of the overall gain G over y and the corresponding derivative using the parameters $[S, \varphi, A, \alpha] = [1000, 0.4, 22, 0.6]$.

The gain factor analysis offers the possibility to explicitly calculate parameter values in combination with the maximum curvature theory in the original system of differential

equations (4.1). Thus, A and α can be explicitly expressed in dependency on the set-point by

$$A = \frac{x_{sp}}{(1 - \mathrm{e}^{-1})} \quad \text{and} \quad \alpha = \frac{1}{y_{sp}}. \tag{4.17}$$

Additionally, x_{sp} and y_{sp} depend solely on S and φ following (4.6) and (4.7). To illustrate the course of x and y in the state space with the parameters A, α substituted using equation (4.17), the inverse of the T-function (4.4) is calculated as

$$y = -\frac{1}{\alpha} \ln\left(\frac{A - x}{A}\right)\Bigg(\tag{4.18}$$

The exemplary hormonal course in the phase space as a result of the previous framework is shown in Fig. 4.5. The identification of the corresponding parameters in the course of calibration will be explained in detail in the applied chapters.

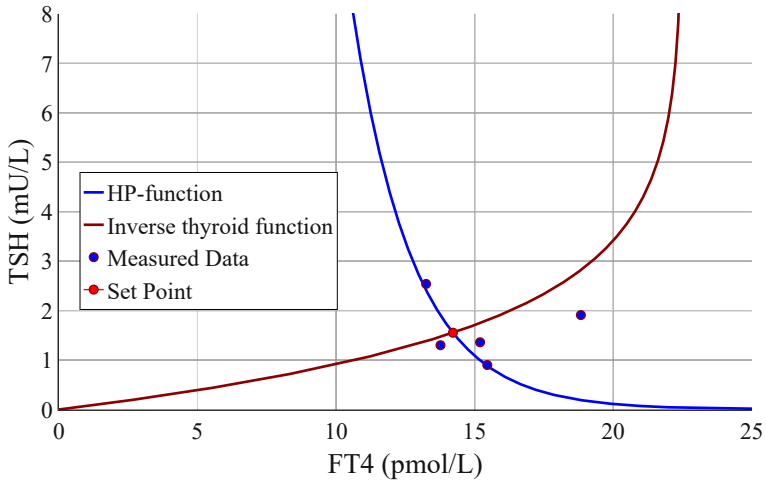

Figure 4.5: Equilibrium curves, set-point and patient data with $x_{sp} = 14.22$, $y_{sp} = 1.55$, $S = 1002.24$, $\varphi = 0.46$, $A = 22.49$, $\alpha = 0.64$.

Figure 4.5 shows that both equilibrium curves intersect at the set-point. The HP-function exhibits an exponential decrease while the inverse of the T-function increases exponentially with increasing FT4.
The gain factor analysis not only provides the possibility to explicitly determine the set-point coordinates and derive dependencies of parameters, but to represent the model (4.1) as a closed-loop control system as shown in Fig. 4.3.

4.1.4 Analysis of the Set-Point Equations

All three approaches explained in detail in previous sections result in explicit expressions of the set-point (x_{sp}, y_{sp}) in dependence of either S and φ or A and α, which can be

summarized to

$$\begin{aligned} x_{sp}^{\text{mch}} &= \frac{\ln(\sqrt{2}S\varphi)}{\varphi} & x_{sp}^{\text{gf}} &= A\,(1-\exp(-1)) & x_{sp}^{\text{mct}} &= A - \frac{1}{\sqrt{2}\alpha} \\ y_{sp}^{\text{mch}} &= \frac{1}{\sqrt{2}\varphi} & y_{sp}^{\text{gf}} &= \frac{1}{\alpha} & y_{sp}^{\text{mct}} &= \frac{\ln(\sqrt{2}A\alpha)}{\alpha}. \end{aligned} \tag{4.19}$$

Combining the set-point derivations explained in detail in 4.1.2 and 4.1.3 seemingly provides the possibility to derive an explicit expression of A and α, since both approaches result in terms representing x_{sp} and y_{sp} in dependence of those two parameters. According to both underlying theories, the expressions should at least not be contradicting. This can be shown by

$$y_{sp}^{\text{gf}} = y_{sp}^{\text{mct}} \quad \Leftrightarrow \quad \frac{1}{\alpha} = \frac{\ln(\sqrt{2}A\alpha)}{\alpha} \quad \Leftrightarrow \quad \ln(\sqrt{2}A\alpha) = 1 \quad \Leftrightarrow \quad \sqrt{2}A\alpha = \exp(1), \tag{4.20}$$

and therefore

$$x_{sp}^{\text{gf}} = A\left(1 - \frac{1}{\sqrt{2}A\alpha}\right) \overset{(4.20)}{=} A\,(1-\exp(-1)) = x_{sp}^{\text{mct}}. \tag{4.21}$$

By additionally using

$$x_{sp}^{\text{gf}} = x_{sp}^{\text{mct}} \quad \Leftrightarrow \quad A\left(1 - \frac{1}{\sqrt{2}A\alpha}\right) = A\,(1-\exp(-1)) \quad \Leftrightarrow \quad \sqrt{2}A\alpha = \exp(1) \tag{4.22}$$

and the resulting relation

$$y_{sp}^{\text{mct}} \overset{(4.22)}{=} \frac{\ln(\exp(1))}{\alpha} = \frac{1}{\alpha} = y_{sp}^{\text{gf}}, \tag{4.23}$$

it follows that

$$x_{sp}^{\text{gf}} = x_{sp}^{\text{mct}} \quad \Leftrightarrow \quad y_{sp}^{\text{gf}} = y_{sp}^{\text{mct}}, \tag{4.24}$$

which, according to the previous analysis, corresponds to

$$x_{sp}^{\text{gf}} = x_{sp}^{\text{mct}} \wedge y_{sp}^{\text{gf}} = y_{sp}^{\text{mct}} \quad \Leftrightarrow \quad \sqrt{2}A\alpha = \exp(1). \tag{4.25}$$

Therefore, it was shown that the relation of the resulting set-points of both section 4.1.2 and 4.1.3 depends solely on the parameters A and α according to (4.25), whereas there are infinite solutions for both parameters.

4.1.5 Sensitivity Analysis

The sensitivity analysis, described in detail in 3.3, is applied to the minimal model to gain information about the contribution of specific parameters to the model output variance. In Fig. 4.6, a matrix containing the Sobol' sensitivity indices of first and second order with respect to the last point of the time-dependent trajectories of the minimal model (4.1) is plotted.

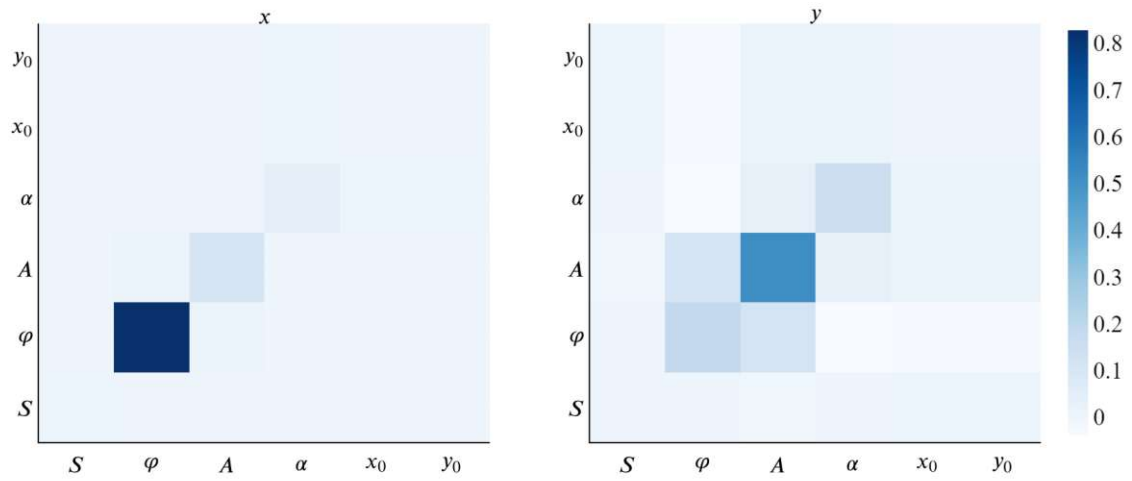

Figure 4.6: Heatmap of Sobol' indices of first and second order of the minimal model for x (left) and y (right). The entries of the diagonal correspond to the indices of first order, the remaining entries represent the second order indices.

As shown in Fig. 4.6, the maximum Sobol' index of first order of x is found for the parameter φ, thus the final point of the corresponding trajectory is most sensitive to the parameter φ. Most of the other parameters do not contribute significantly to the model output variance. Especially, there is no significant influence of the interaction of any parameters according to the low value of the Sobol' index of second order. Compared to φ, the Sobol' index of the parameters A and α indicate a smaller influence on the model output variance.
In contrast to the results of x, Sobol' indices of second order significantly larger than zero are found for the final point of the trajectory of y. Figure 4.6 indicates that the interaction between A and φ as well as A and α significantly contribute to the model output variance. Similar to the sensitivity results of x, the parameters φ, A and α have the highest Sobol' index of first order, while A has the maximum influence on the final point of the y trajectory. The parameter S and the initial values (x_0, y_0) do not contribute to the model output variance with respect to the final point of both trajectories according to Sobol' index.
Thus, the results of the minimal model presented in 6 are expected to show a higher variance of the last point of the trajectories with respect to φ, A and α compared to S or parameter interactions. Sensitivity analysis implies the possibility to further restrict the interval that determines the possible range of S during parameter identification for runtime or computational cost efficiency.

4.1.6 Parameter Identification

The parameter values for the model are determined in the course of a calibration using patient data described in detail in section 2.3. Two calibration approaches are pursued.
The first approach refers to a direct calibration of the time-dependent course of both $x(t)$ and $y(t)$ determined by the system of differential equations (4.1). This approach is equiv-

alent to the procedure described in section 3.4 with $\tilde{z}(t,\theta) = (x(t,\theta), y(t,\theta)) \in \mathbb{R}^2$ and $\theta = (S, \varphi, A, \alpha) \in \mathbb{R}^4$. Thus, the aim of this parameter identification is to find parameters with minimal deviation to the patient data and minimize the corresponding objective function given by (3.17).

The second approach is based on the results presented in section 4.1.3 and describes the calibration of the function $y(x)$ given by (4.3) in the state space resulting in parameters S and φ. Subsequently, the respective set-point coordinates are calculated based on the curvature of $y(x)$ with the optimal parameters S and φ and the parameters A and α are then derived explicitly according to (4.17). This represents a calibration of a function that is not time-dependent, thus the problem formulation needs to be adapted with respect to the general process of parameter identification described in section 3.4.
The model is given by $y(x,\theta)$ with $\theta = (S, \varphi)$ according to

$$y(x) = \frac{S}{\exp(\varphi x)}. \tag{4.26}$$

It is determined by the equilibrium equation of model (4.1) and thus only depends implicitly on the system of differential equations. The reference data used for the calibration consists of pairs (x_l, y_l) with $l = 1, ..., n$ and the corresponding model evaluation $y(x_l)$. Since the calibration is based on the course of only one variable, the error does not need to be normalized, resulting in an objective function defined as

$$\xi(\theta) = \frac{1}{n} \sum_{l=1}^{n} (y(x_l, \theta) - y_l)^2. \tag{4.27}$$

Therefore, two parameters of model (4.1) are identified by the use of a calibration algorithm while the other two are calculated directly based on the previously derived mathematical framework.

4.2 A Unified Model of the Thyroid Hormone Regulation

The mathematical model described by [YTH+21] is used as an additional supplementary and comparative description of the HPT system. In line with the model presented in section 4.1, it consists of two differential equations describing the temporal change of [TSH] and [FT4], respectively, by including their mutual influence as negative feedback control mechanism and the endogenous reduction of both hormones. In order to represent disease states related to the thyroid gland, the parameter G was introduced to account for the use of medication. Additionally, the model also includes a set-point defined as the hormonal equilibrium corresponding to an euthyroid state. This set-point is described explicitly by the parameters U for [FT4] and indirectly by p_1 for [TSH], which are included directly in the system.

The model describes the HPT regulatory system in a euthyroid state by the following system of differential equations

$$\begin{aligned} \frac{\mathrm{d}[\mathrm{TSH}]}{\mathrm{d}t} &= p_1 - \frac{p_1([\mathrm{FT4}] - U)}{s_1 + [\mathrm{FT4}]} - d_1[\mathrm{TSH}], \\ \frac{\mathrm{d}[\mathrm{FT4}]}{\mathrm{d}t} &= \frac{p_2(t)[\mathrm{TSH}]}{s_2 + [\mathrm{TSH}]} - d_2[\mathrm{FT4}] + G. \end{aligned} \tag{4.28}$$

The parameter G describes the amount of increased or decreased thyroxine levels per unit time caused by thyroid medication intake.
In [YTH+21], the euthyroid set-point for [FT4] is considered as individual. Complementary, the parameter p_1 is the standard rate of release of [TSH] from the pituitary gland when [FT4] reaches its set-point value U. For further analysis of the introduced set-point, the so-called TSH-secretion-function $f([\mathrm{FT4}])$ is defined as

$$f([\mathrm{FT4}]) = p_1 - \frac{p_1([\mathrm{FT4}] - U)}{s_1 + [\mathrm{FT4}]} = p_1 \frac{s_1 + U}{s_1 + [\mathrm{FT4}]}. \tag{4.29}$$

It follows immediately that $f(U) = p_1$, describing a pituitary level-off at a standard release rate of [TSH] when the release rate of [FT4] is optimal. In addition, the pituitary gland secretes more [TSH] in response to a lower amount of secreted [FT4] and vice versa, thus depending on the ratio of [FT4] and U. The TSH-secretion-function represents this behavior by

$$f([\mathrm{FT4}]) < p_1 \quad \text{if} \quad [\mathrm{FT4}] > U, \tag{4.30}$$

$$f([\mathrm{FT4}]) > p_1 \quad \text{if} \quad [\mathrm{FT4}] < U, \tag{4.31}$$

as the quotient in (4.29) is either smaller or larger than one. It is also assumed that the euthyroid set-point is equal to the model equilibrium. Therefore, for a euthyroid state, the model parameter p_2 can be expressed by the other parameters. First, the equilibrium state for [FT4], denoted by $[\mathrm{FT4}]^*$, is calculated by $\frac{\mathrm{d}[\mathrm{FT4}]}{\mathrm{d}t} = 0$ resulting in

$$[\mathrm{FT4}]^* = \frac{p_2\,[\mathrm{TSH}]^*}{d_2(s_2 + [\mathrm{TSH}]^*)} \overset{!}{=} U. \tag{4.32}$$

Analogously, the equilibrium for [TSH], denoted as $[\mathrm{TSH}]^*$, is calculated to be

$$[\mathrm{TSH}]^* = \frac{p_1(s_1 + U)}{d_1(s_1 + [\mathrm{FT4}]^*)} = \frac{p_1}{d_1}. \tag{4.33}$$

By inserting (4.33) into (4.32) and rearrange the equation according to the objective parameter, p_2 can be described explicitly as

$$p_2 = d_2 U \left(1 + \frac{d_1 s_2}{p_1}\right)\left(\tag{4.34}$$

4.2.1 Applicability of the Maximum Curvature Theory

The previously presented maximum curvature theory, originally introduced in the context of model (5.1), states that the point of maximum curvature of the HP-function corresponds to the point of maximum sensitivity of the pituitary. Therefore, it can be used to describe the set-point explicitly in dependence of other model parameters. Thus, the maximum curvature theory is applied to the model (4.28), which is also an autonomous system of differential equations. The results are compared with the explicit representation of the set-point of [FT4] by the parameter U and p_1, the standard release rate of [TSH] at the set-point. In [YTH+21], the definition of parameter p_2 varies in dependence on the thyroidal state - euthyroid, hypothyroid or hyperthyroid. For this approach, only the euthyroid state is considered due to the definition of the set-point with respect to a euthyroid state. This is also the reason why $G = 0$ is required. Here and in the following, model (4.28) is additionally reformulated by substituting $y = [\text{TSH}]$ and $x = [\text{FT4}]$ due to readability purposes resulting in

$$\begin{aligned} \frac{\mathrm{d}y}{\mathrm{d}t} &= p_1 - \frac{p_1(x-U)}{s_1+x} - d_1 y, \\ \frac{\mathrm{d}x}{\mathrm{d}t} &= \frac{p_2 y}{s_2+y} - d_2 x. \end{aligned} \tag{4.35}$$

Application of the Maximum Curvature Theory to the TSH-Function

The TSH-function is defined equivalently to the HP-function (4.3) of model (4.1). It can be derived by determining the steady state equation for y defined by $\frac{\mathrm{d}y}{\mathrm{d}t} = 0$ leading to the TSH-function

$$y = \frac{1}{d_1}\left(\frac{p_1(s_1+U)}{(s_1+x)}\right)\left(\tag{4.36}$$

By inserting the first and second derivative of (4.36) in (3.1), the corresponding curvature K_y is determined to be

$$K_y = \frac{2p_1(s_1+U)}{d_1(s_1+x)^3}\left(\left(+\frac{p_1^2(s_1+U)^2}{d_1^2(s_1+x)^4}\right)^{-\frac{3}{2}}. \tag{4.37}$$

The set-point can then be calculated by $\frac{\mathrm{d}K_y}{\mathrm{d}x} = 0$ leading to the four solutions

$$x_{1,2,3,4} = \frac{\pm\sqrt{\pm d_1 p_1(s_1+U)} - d_1 s_1}{d_1}. \tag{4.38}$$

Since all included parameters are positive and the set-point candidate for x must be a positive real number, it follows that

$$x_{sp} = \frac{\sqrt{d_1 p_1(s_1+U)} - d_1 s_1}{d_1}, \tag{4.39}$$

and furthermore

$$y_{sp} \overset{(4.36)}{=} \sqrt{\left(\frac{p_1(s_1+U)}{d_1}\right.}. \tag{4.40}$$

Thus, an explicit expression of the set-point coordinates of x and y could have been derived and the maximum curvature theory is at least applicable to the TSH-function of model (4.28).

Application of the Maximum Curvature Theory to the FT4-Function

In line with previous approaches, the maximum curvature theory is also applied to the so-called FT4-function of model (4.35) in order to determine the corresponding point of maximum sensitivity. The FT4-function is derived by $\frac{\mathrm{d}x}{\mathrm{d}t} = 0$ as

$$x = \frac{1}{d_2}\left(\frac{p_2 y}{(s_2+y)}\right)\left(\tag{4.41}$$

The curvature of x is determined using its first and second derivative and (3.1) as

$$K_x = -\frac{2p_2 s_2}{d_2(s_2+y)^3} \quad \left(1+\frac{p_2 s_2}{d_2(s_2+y)^2}\right)^2\Bigg)^{-\frac{3}{2}}. \tag{4.42}$$

By calculating the first derivative of K_x with respect to y and solving the equation $\frac{\mathrm{d}K_x}{\mathrm{d}y} = 0$, the candidates for the y-coordinate of the set-point can be derived as

$$y_{1,2,3,4} = \frac{-\sqrt{d_2}s_2 \pm \sqrt{\pm p_2 s_2}}{\sqrt{d_2}}. \tag{4.43}$$

The set-point and all the included parameters are required to be real positive numbers, therefore is follows that

$$y_{sp} = \frac{-\sqrt{d_2}s_2 + \sqrt{p_2 s_2}}{\sqrt{d_2}}, \tag{4.44}$$

and as a consequence

$$x_{sp} = \frac{p_2}{d_2} - \frac{s_2}{\sqrt{d_2 p_2 s_2}}. \tag{4.45}$$

Thus, the maximum curvature theory applied to the FT4-function leads to a unique, explicit expression of the set-point. The significance of the theory applied to this model in physiological terms can be further investigated in the context of data-based simulation of the course of both corresponding hormones.

4.2.2 Closed-Loop Control System and Gain Factor Analysis

In order to represent model (4.28) as a closed-loop system in line with Fig.4.3, the framework presented in section 3.4 is applied. This not only offers the possibility to specify the gain factor for both the TSH- and FT4-complexes, but according to [LG14] is an approach to determine an explicit representation of the set-point using the optimal overall gain factor. The gain G_{TSH} is defined by the derivative of equation (4.36) with respect to x, which leads to

$$G_{TSH} = \frac{\mathrm{d}y}{\mathrm{d}x} = -\frac{p_1(s_1+U)}{d_1(s_1+x)^2}. \tag{4.46}$$

Since the optimal gain factor in the context of set-point specification in [LG14] is defined using the derivative with respect to y, G_{TSH} must be reformulated using

$$\frac{1}{(s_1+x)} \overset{(4.36)}{=} \frac{d_1 y}{p_1(s_1+U)}, \tag{4.47}$$

and (4.36) as

$$G_{TSH} = -\underbrace{\frac{p_1(s_1+U)}{d_1(s_1+x)}}_{=y}\frac{1}{(s_1+x)} = -\frac{d_1 y^2}{p_1(s_1+U)}. \tag{4.48}$$

Analogously, the gain of the FT4-complex can be determined based on (4.41), the equilibrium equation of x, by

$$G_{FT4} = \frac{\mathrm{d}x}{\mathrm{d}y} = \frac{p_2 s_2}{d_2(s_2+y)^2}. \tag{4.49}$$

Since G_{FT4} depends only on y, no further transformations are necessary. Thus, based on these terms, the optimal overall gain factor is calculated based on $\frac{\mathrm{d}G}{\mathrm{d}y} = 0$ with

$$\frac{\mathrm{d}G}{\mathrm{d}y} = \frac{\mathrm{d}}{\mathrm{d}y}|G_{TSH}G_{FT4}| = \frac{\mathrm{d}}{\mathrm{d}y}\left(\frac{d_1 y^2 p_2 s_2}{p_1(s_1+U)d_2(s_2+y)^2}\right) = \frac{2d_1 p_2 s_2^2 y}{p_1(s_1+U)d_2(s_2+y)^3}. \tag{4.50}$$

Setting this equation to zero is only solvable for $y = 0$ leading to set-point coordinates of $(x_{sp}, y_{sp}) = (0, 0)$, which are independent of the model parameters. This result contradicts the physiological definition of the set-point being individual for every patient. Therefore, the theory of an optimal gain factor does not result in explicit terms of the set-point coordinates depending on the parameters when applied to model (4.28). The theory yet provides the possibility to represent the model as a closed-loop control system based on the calculated individual gain factors.

4.2.3 Sensitivity Analysis

A sensitivity analysis provides information about the contribution of parameters to the modoutput variance restricted to the last point of the trajectories.
The results of the sensitivity analysis, derived theoretically in section 3.3, applied to the unified model 4.35 are shown in Fig. 4.7.

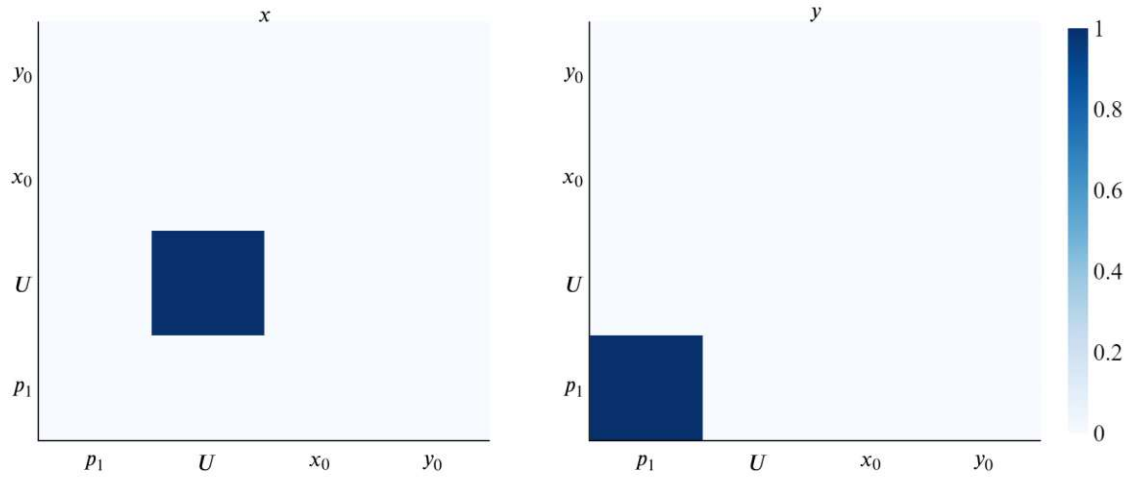

Figure 4.7: Heatmap of Sobol' indices of first and second order of the unified model for x (left) and y (right). The entries of the diagonal correspond to the indices of first order, the remaining entries represent the second order indices.

The Sobol's indices indicate that the parameter U contributes most to the variance of the final point of the x trajectory in correspondence to the definition of U. In line with this result, the maximum Sobol' index of the y trajectory is associated with the parameter p_1. All other parameters or pairwise interactions do not show a significant influence on the model output variance. Thus, the largest contribution to the variance of last point of both trajectories is associated with the parameters determining the set-point of both curves.

4.2.4 Parameter Identification

In order to obtain more information about the model, the previous theoretical analysis is extended to the practical approach of calibration to patient data, which is presented in chapter 6. As a basis, the problem must be formulated in terms of parameter identification as described in detail in section 3.4.
The approach corresponds a direct calibration of the time-dependent course of both $x(t)$ and $y(t)$ determined by the system of differential equations (4.35). This approach is equivalent to the procedure described in section 3.4 with

$$\tilde{z}(t,\theta) = (x(t,\theta), y(t,\theta)) \in \mathbb{R}^2 \qquad \text{and} \qquad \theta = (p_1, s_1, U) \in \mathbb{R}^3. \tag{4.51}$$

Thus, the aim of this parameter identification is to minimize the corresponding objective function given by (3.17).

The values for the remaining parameters are fixed based on their description resulting in $s_2 = 0.0021, d_1 = 16.635, d_2 = 0.09921$ and the respective values are determined in [YTH+21] as well as in [Pan11]. The parameter p_2 can be calculated depending on the others.
The calibration of the models presented in this chapter provides more information about the system dynamics and especially the set-point. In addition to the explicit equations of the set-point coordinates, it is contextualized with stability behavior of the models in the course of a qualitative analysis.

5 Qualitative Analysis

An analytical investigation of mathematical models allows statements to be made about the general short- and long-term behavior, stability and robustness before they are calibrated in the course of a parameter identification. In this chapter, the two models presented in chapter 4 are analyzed in terms of equilibrium points and the corresponding local and global stability by means of theoretical and graphical approaches. In order to obtain further information on the correlation of the set-point equations of the model presented in section 4.1, which were derived using maximum curvature theory and gain factor analysis, the stability of these explicit set-point equations is also considered.

5.1 Stability Analysis of the Minimal Model of the HPT Axis

Direction fields show the general long-term course of trajectories of a system of differential equations. Thus, in the course of a graphical analysis, equilibrium points and their local and global stability can be identified.
An exemplary direction field of the system of differential equations (4.1) including two sample trajectories, shown in Fig. 5.1, suggests the existence of an asymptotically stable equilibrium point.
The system (4.1) is a nonlinear 2-dimensional autonomous system given by

$$\begin{aligned} \frac{\mathrm{d}x}{\mathrm{d}t} &= A - \frac{A}{\exp(\alpha y)} - x := f_1(x, y), \\ \frac{\mathrm{d}y}{\mathrm{d}t} &= \frac{S}{\exp(\varphi x)} - y := f_2(x, y). \end{aligned} \tag{5.1}$$

5.1.1 Local Stability Analysis

This section is concerned with the local stability analysis of an autonomous system,

$$u'(t) = f(u(t)), \tag{5.2}$$

with $f : D \to \mathbb{R}^d$ and $D \subseteq \mathbb{R}^d$, based on the analysis of the Jacobian matrix $\mathbf{J}$ in the course of the principle of linearized stability. The mathematical framework, introduced shortly in this section, is based on and explained in more detail in [HD19].

Definition 8. *A point $u^* \in D$ with $f(u^*) = 0$ is called a critical or equilibrium point of f.*

The stability of an autonomous system around an equilibrium point can then be analyzed by linearization of the respective system using the Taylor series expansion of first order around the equilibrium as a development point.

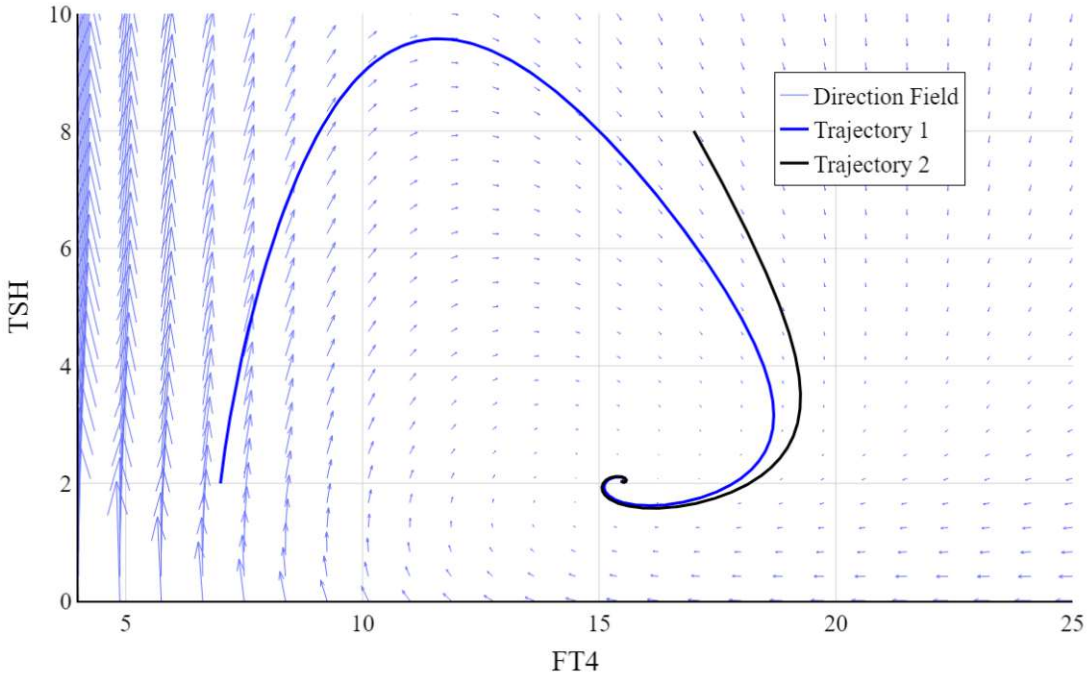

Figure 5.1: Direction field of model (4.1) including two sample trajectories. The initial value for trajectory 1 is $[7, 2]$ and for trajectory 2 it is $[17, 8]$. The exemplary parameter set was chosen with $[S, \varphi, A, \alpha] = [1000, 0.4, 22, 0.6]$.

By omitting the remainders obtained during the Taylor series expansion, this approach leads to the linear system of differential equations with constant coefficients

$$u'(t) \approx \mathbf{J}_f(u^*)u(t). \tag{5.3}$$

Depending on the characteristics of the Jacobian matrix $\mathbf{J}_f(u^*)$ of f evaluated at the equilibrium point u^*, its stability properties can be derived based on the trace according to the following theorem.

Theorem 1. ***(Principle of linearized stability)*** *Let $D \subseteq \mathbb{R}^d$ be an open set and a function $f \in C^1(D, \mathbb{R}^d)$. If u^* is a critical point of f, then it holds that*

1. *If $tr(\mathbf{J}_f(u^*)) < 0$, then u^* is asymptotically stable.*
2. *If $tr(\mathbf{J}_f(u^*)) > 0$, then u^* is unstable.*

In line with [Heu91], equilibrium points of a 2-dimensional system of differential equations can be further classified according to the eigenvalues λ_1, λ_2 of the Jacobian $\mathbf{J}_f(u^*)$ due to the following lemma. It is reduced to cases where $\lambda_1, \lambda_2 \in \mathbb{C}$ as only such cases are present within the models considered in this work.

Lemma 1. *Let $\lambda_{1,2} = \alpha \pm \mathrm{i}\beta$ be conjugated complex eigenvalues of $\boldsymbol{J}_f(u^*)$.*

- *If $\alpha < 0$ and $\beta \neq 0$, u^* is an asymptotically stable spiral.*
- *If $\alpha > 0$ and $\beta \neq 0$, u^* is an unstable spiral.*
- *If $\alpha = 0$ and $\beta \neq 0$, u^* is a stable center.*

The local qualitative analysis of model (5.1) is based on several approaches including the determination of the general equilibrium point and the set-point equations derived in section 4.1. Following the general approach to determine the equilibrium point of (5.1) results in

$$\begin{aligned} \frac{\mathrm{d}y}{\mathrm{d}t} = 0 \quad &\Rightarrow \quad y^* = S\exp(-\varphi x^*) \\ \frac{\mathrm{d}x}{\mathrm{d}t} = 0 \quad &\Rightarrow \quad x^* = A\left(1 - \frac{1}{\exp(\alpha y^*)}\right) = A\left(1 - \frac{1}{\exp(\alpha S\exp(-\varphi x^*))}\right) \end{aligned} \tag{5.4}$$

These equations cannot be solved analytically to obtain an explicit expression for both x^* and y^*, but the previously derived equations for the set-point can be analyzed in the same context.

To analyze the qualitative behavior of the system of differential equations (5.1) with respect to the derived set-point, it must be assumed that all equations summarized in (4.19) equally represent the same set-point. Otherwise, the theoretical analysis could not be applied since the differential equation for x depends on A and α while the differential equation for y depends on S and φ. This implies that the set-point expression including the respective two matching parameters has to be chosen in order to apply the previously described framework for a qualitative analysis of (5.1). This assumption corresponds to the analysis performed in section 4.1.4 and the definition of the set-point to represent the unique individual hormonal equilibrium.
For readability purposes, the set-point equations, derived based on the maximum curvature theory applied to the HP- and the T-function and the gain factor analysis are repeated in this section. They are given as

$$\begin{aligned} x_{sp}^{\mathrm{mch}} &= \frac{\ln(\sqrt{2}S\varphi)}{\varphi} & x_{sp}^{\mathrm{gf}} &= A\left(1 - \exp(-1)\right) & x_{sp}^{\mathrm{mct}} &= A - \frac{1}{\sqrt{2}\alpha} \\ y_{sp}^{\mathrm{mch}} &= \frac{1}{\sqrt{2}\varphi} & y_{sp}^{\mathrm{gf}} &= \frac{1}{\alpha} & y_{sp}^{\mathrm{mct}} &= \frac{\ln(\sqrt{2}A\alpha)}{\alpha}. \end{aligned} \tag{5.5}$$

Proposition 1. *The set-point, derived in section 4.1.1 and 4.1.3 using the maximum curvature theory applied to the HP-function and the gain factor analysis, is an asymptotically stable equilibrium of* (5.1).

Proof. First, the set-point is an equilibrium of (5.1) according to

$$\begin{aligned} \frac{\mathrm{d}x}{\mathrm{d}t} &= A - \frac{A}{\exp(\alpha y_{sp}^{\mathrm{gf}})} - x_{sp}^{\mathrm{gf}} = A\left(1 - \exp(-1)\right) - A\left(1 - \exp(-1)\right) = 0, \\ \frac{\mathrm{d}y}{\mathrm{d}t} &= \frac{S}{\exp(\varphi x_{sp}^{\mathrm{mch}})} - y_{sp}^{\mathrm{mch}} = \frac{S}{\exp(\ln(\sqrt{2}S\varphi))} - \frac{1}{\sqrt{2}\varphi} = 0. \end{aligned} \tag{5.6}$$

For the stability analysis, the Jacobian matrix is computed. It can be derived and evaluated at (x_{sp}, y_{sp}) following

$$\mathbf{J}(x_{sp}^{\text{mch}}, y_{sp}^{\text{gf}}) = \begin{pmatrix} -1 & A\alpha\exp(-\alpha y) \\ S\varphi\exp(-\varphi x) & -1 \end{pmatrix}_{(x_{sp}^{\text{mch}}, y_{sp}^{\text{gf}})} = \begin{pmatrix} -1 & A\alpha\exp(-1) \\ -\sqrt{2} & -1 \end{pmatrix} \tag{5.7}$$

To finally analyze the stability, the corresponding eigenvalues are calculated by

$$|\mathbf{J} - \lambda\mathbf{E}| = (1+\lambda)^2 + \alpha A\sqrt{2}\exp(-1) = 0. \tag{5.8}$$

It follows that

$$\lambda_{1,2} = -1 \pm \sqrt{-\alpha A\sqrt{2}\exp(-1)} = -1 \pm \mathrm{i}\sqrt{\alpha A\sqrt{2}\exp(-1)} \in \mathbb{C}. \tag{5.9}$$

Thus, the eigenvalues of the Jacobian matrix are complex since $A, \alpha > 0$ with $\mathrm{Re}(\lambda_{1,2}) < 0$. This leads to the conclusion that the set-point is a spiral sink and therefore asymptotically stable, which corresponds to the behavior that can be observed in the phase portrait shown in Fig. 5.1. □

To further evaluate the assumption of an equal set-point representation, the same framework is analogously applied to the results of 4.1.1 and 4.1.2.

Proposition 2. *The set-point, derived as a result of 4.1.1 and 4.1.2, is an asymptotically stable equilibrium of* (5.1).

Proof. Substituting x and y by the formulas for $(x_{sp}^{\text{mch}}, y_{sp}^{\text{mch}})$ and $(x_{sp}^{\text{mct}}, y_{sp}^{\text{mct}})$ in system (5.1), respectively, likewise results in an equilibrium equation according to

$$\begin{aligned} \frac{\mathrm{d}x}{\mathrm{d}t} &= A - \frac{A}{\exp(\alpha y_{sp}^{\text{mct}})} - x_{sp}^{\text{mct}} = A - \frac{A}{\exp(\ln(\sqrt{2}A\alpha))} - \left(A - \frac{1}{\sqrt{2}\alpha}\right) = 0, \\ \frac{\mathrm{d}y}{\mathrm{d}t} &= \frac{S}{\exp(\varphi x_{sp}^{\text{mch}})} - y_{sp}^{\text{mch}} = 0. \end{aligned} \tag{5.10}$$

The Jacobian is evaluated at (x_{sp}, y_{sp}) as

$$\mathbf{J}(x_{sp}^{\text{mch}}, y_{sp}^{\text{mct}}) = \begin{pmatrix} -1 & A\alpha\exp(-\alpha y) \\ S\varphi\exp(-\varphi x) & -1 \end{pmatrix}_{(x_{sp}^{\text{mch}}, y_{sp}^{\text{mct}})} = \begin{pmatrix} -1 & \sqrt{2} \\ -\sqrt{2} & -1 \end{pmatrix} \tag{5.11}$$

The corresponding eigenvalues are then calculated based on the characteristic polynomial following

$$|\mathbf{J} - \lambda\mathbf{E}| = \lambda^2 + 2\lambda + 3 = 0. \tag{5.12}$$

Solving this equation leads to

$$\lambda_{1,2} = -1 \pm \sqrt{-2} = -1 \pm \mathrm{i}\sqrt{2} \in \mathbb{C}. \tag{5.13}$$

According to the complex eigenvalues, the equilibrium points is corresponds to an asymptotically stable spiral sink. Therefore, it can be concluded that this representation of the set-point is also an equilibrium point of the system of differential equations exhibiting the same stability characteristics. □

5.1.2 Global Stability Analysis

Since the previous analysis only proves the local stability, the following approach is used to furthermore prove the existence of an equilibrium and its global stability based on the Dulac-Bendixon-Criterion and the Poincaré-Bendixon-Theorem. For this approach, the overall framework presented in [YTH+21] is applied to model (5.1).

Theorem 2. ***(Dulac-Bendixon-Criterion)***
Let $Z \subseteq X$ be open and simply connected. Assume the following:

1. *The functions f_1 and f_2 are continuously differentiable on Z.*
2. *There exists a function $D : Z \to R$, continuously differentiable on Z, such that*

$$\frac{\partial(Df_1)}{\partial x} + \frac{\partial(Df_2)}{\partial y} \tag{5.14}$$

is either strictly positive almost everywhere on Z or strictly negative almost everywhere on Z.

Then Z contains no periodic orbits or graphics. [Mar15]

Theorem 2 is applied to system (5.1) in the following Lemma 2.

Lemma 2. *The system* (5.1) *has no periodic orbits or graphics in $\mathbb{R}^2_+$.*

Proof. Let $Z = \mathbb{R}^2_+$ that is open and simply connected. By choosing $D \equiv 1$, it follows that

$$\frac{\partial(Df_1)}{\partial x} + \frac{\partial(Df_2)}{\partial y} = -2 < 0. \tag{5.15}$$

Thus, according to the Dulac-Bendixon-Criterion, the model has neither periodic orbits nor graphics. □

This preliminary work will be used in combination with the Poincaré-Bendixon-Theorem given in Theorem 3, for which the additional Definition 9 is needed. Let $u(t) = (x(t), y(t))$ be a solution curve with initial condition $u_0 = (x(0), y(0))$.

Definition 9. *The omega limit set of the point u_0, denoted by $\omega(u_0)$, consists of all points $a \in \mathbb{R}^2$ for which there is a sequence $t_j, j = 1, 2, ...,$ such that $u(t_j) \to a$ for $t_j \to \infty$. [Mar15]*

Theorem 3. ***(Poincaré-Bendixon-Theorem)*** *Assume that $X \subseteq \mathbb{R}^2$, where X is an open set, contains only finitely many equilibria. Let $u(t)$ be a solution in X that is defined and bounded on $[0, \infty)$ with $\omega(u_0) \subseteq X$. Then one of the following holds:*

1. *$\omega(u_0)$ consists of an equilibrium.*
2. *$\omega(u_0)$ is a periodic orbit.*
3. *$\omega(u_0)$ a graphic. [Mar15]*

Lemma 3. *All trajectories of the model* (5.1) *are constrained in a bounded region of* $\mathbb{R}^2_+$.

Proof. The model given in (5.1) can be rewritten as

$$\begin{aligned}\frac{\mathrm{d}}{\mathrm{d}t}(x+\alpha) &= A - A\mathrm{e}^{-\alpha(y+\varphi)}\mathrm{e}^{\alpha\varphi} - (x+\alpha) + \alpha,\\ \frac{\mathrm{d}}{\mathrm{d}t}(y+\varphi) &= S\mathrm{e}^{-\varphi(x+\alpha)}\mathrm{e}^{\alpha\varphi} - (y+\varphi) + \varphi.\end{aligned} \tag{5.16}$$

Substituting the variables $u = y + \varphi$ and $v = x + \alpha$ results in

$$\frac{\mathrm{d}v}{\mathrm{d}t} = A - A\mathrm{e}^{-\alpha u}\mathrm{e}^{\alpha\varphi} - v + \alpha, \tag{5.17}$$

$$\frac{\mathrm{d}u}{\mathrm{d}t} = S\mathrm{e}^{-\varphi v}\mathrm{e}^{\alpha\varphi} - u + \varphi. \tag{5.18}$$

It will now be shown that $\liminf_{t\to\infty} v(t) > 0$ and $\liminf_{t\to\infty} u(t) > 0$ and the limes superior is restricted for both $u(t), v(t)$ and $t \to \infty$.

1. It will be shown that $\limsup_{t\to\infty} v(t) \leq A + \alpha < \infty$. Based on the product rule, equation (5.17) can be rewritten as

$$\frac{\mathrm{d}}{\mathrm{d}t}(\mathrm{e}^t v(t)) = -A\mathrm{e}^{-\alpha u+\alpha\varphi+t} + \mathrm{e}^t(A+\alpha). \tag{5.19}$$

   By integrating the equation with respect to t, it follows that

$$\mathrm{e}^t v(t) - v(0) = -\int_0^t \frac{A\mathrm{e}^{\alpha\varphi+s}}{\mathrm{e}^{\alpha u}}\,\mathrm{d}s + \int_0^t \mathrm{e}^s(A+\alpha)\,\mathrm{d}s \tag{5.20}$$

$$= -\int_0^t \frac{A\mathrm{e}^{\alpha\varphi+s}}{\mathrm{e}^{\alpha u}}\,\mathrm{d}s + \mathrm{e}^t(A+\alpha)(1-\mathrm{e}^{-t}) \tag{5.21}$$

$$< \mathrm{e}^t(A+\alpha)(1-\mathrm{e}^{-t}). \tag{5.22}$$

   Thus,

$$v(t) < (A+\alpha)(1-\mathrm{e}^{-t}) + \mathrm{e}^{-t}v(0), \tag{5.23}$$

   which implies

$$v^* := \limsup_{t\to\infty} v(t) \leq A + \alpha < \infty. \tag{5.24}$$

2. Analogously, it can be proven that $\liminf_{t\to\infty} u(t) \geq \varphi > 0$ by reformulating equation (5.18) such that

$$\frac{\mathrm{d}}{\mathrm{d}t}(\mathrm{e}^t u(t)) = S\mathrm{e}^{-\varphi v+\alpha\varphi+t} + \mathrm{e}^t\varphi. \tag{5.25}$$

By again integrating both sides of the equation with respect to t, it follows that

$$e^t u(t) - u(0) = \int_0^t \frac{S e^{\alpha\varphi+s}}{e^{\varphi v}} \, ds + \int_0^t e^s \varphi \, ds \tag{5.26}$$

$$> e^t \varphi (1 - e^{-t}). \tag{5.27}$$

Therefore,

$$u(t) > \varphi(1 - e^{-t}) + e^{-t} u(0), \tag{5.28}$$

which finally leads to

$$u_* := \liminf_{t\to\infty} u(t) \geq \varphi > 0. \tag{5.29}$$

3. To show that $v_* := \liminf_{t\to\infty} v(t) > 0$, let $O := \{(v(t), u(t) : 0 \leq t < \infty)\}$ be an orbit lying in the first quadrant. Let $Z := \{0 \leq t_1 < t_2 < ... < t_n < ...\}$ be the sequence of points in $[0, \infty)$ such that $\dot{v}(t_j) = 0$ for $j = 1, 2, ...$

   It holds that $\inf_{t\geq 0} v(t) = \min\{v(0), v(t_1), ..., v(t_n), ...\}$. Since the equilibrium is a spiral point, Z is an infinite set which implies that (t_n) is an increasing sequence tending to ∞.

   Additionally, let there be an $\epsilon > 0$ close to zero such that $\varphi - \epsilon < \varphi \leq u_*$. Such an ϵ exists since $\varphi > 0$. Therefore, let $\bar{u}$ be chosen such that $\varphi - \epsilon < \bar{u} < u_*$ and let $\bar{v}$ be the intersection of the vertical line $u = \bar{u}$ and the hyperbola $v = -Ae^{-\alpha u} e^{\alpha\varphi} + A + \alpha$. Since $\bar{u} > \varphi - \epsilon$, it follows that

$$\bar{v} = -Ae^{-\alpha\bar{u}} e^{\alpha\varphi} + A + \alpha > -Ae^{-\alpha(\varphi-\epsilon)} e^{\alpha\varphi} + A + \alpha = -Ae^{\alpha\epsilon} + A + \alpha \tag{5.30}$$

   The parameter α defines the decay rate with respect to equation (5.17). Therefore, it holds that $\alpha < 1$ and additionally

$$\bar{v} > -Ae^{\alpha\epsilon} + A + \alpha \underset{\epsilon\to 0}{\longrightarrow} \alpha > 0. \tag{5.31}$$

   Since $\bar{u} < u_*$, there exists an $\bar{t}$ such that $u(t) > \bar{u}$, $\forall t_j \geq \bar{t}$. This implies that the orbit $O_{\bar{t}} := \{(v(t), u(t)) : \bar{t} \leq t < \infty\}$ lies on the right hand side of the vertical line $u = \bar{u}$. Therefore it follows that the intersections of $O_{\bar{t}}$ and the hyperbola $v = -Ae^{-\alpha u} e^{\alpha\varphi} + A + \alpha$ all have their v-coordinates greater than $\bar{v}$. Thus,

$$v(t_j) \geq \bar{v} \quad \forall t_j \geq \bar{t}. \tag{5.32}$$

   Let j_0 be an index chosen such that $t_j \geq \bar{t}\ \forall j \geq j_0$. Then it can be concluded that

$$\inf_{t\geq 0} v(t) = \min\{v(0), v(t_1), ..., v(t_{j_0})\} > \bar{y} > 0. \tag{5.33}$$

4. Finally, it can be shown that $\limsup_{t\to\infty} u(t) < \infty$ by using the already proven properties. Since $v_* > 0$ and $v^* < \infty$, v_0 can be chosen such that $0 < v_0 < v^*$ is fulfilled.

Thus, there exists some t^* such that $\forall t \geq t^* : v_0 < v(t)$. Similar to previous approaches, $u(t)$ can be estimated following

$$\frac{\mathrm{d}}{\mathrm{d}t}(\mathrm{e}^t u(t)) = S\mathrm{e}^{-\varphi v + \alpha\varphi + t} + \mathrm{e}^t\varphi \tag{5.34}$$

$$\Leftrightarrow \mathrm{e}^t u(t) = u(0) + \int_0^t \frac{S\mathrm{e}^{\alpha\varphi+s}}{\mathrm{e}^{\varphi v}}\,\mathrm{d}s + \int_0^t \mathrm{e}^s\varphi\,\mathrm{d}s \tag{5.35}$$

$$\Leftrightarrow \mathrm{e}^t u(t) = u(0) + \int_0^{t^*} \frac{S\mathrm{e}^{\alpha\varphi+s}}{\mathrm{e}^{\varphi v}}\,\mathrm{d}s + \int_{t^*}^t \frac{S\mathrm{e}^{\alpha\varphi+s}}{\mathrm{e}^{\varphi v}}\,\mathrm{d}s + \int_0^t \mathrm{e}^s\varphi\,\mathrm{d}s. \tag{5.36}$$

According to the prior considerations, by using $\mathrm{e}^{v_0} < \mathrm{e}^{v(t)}$ for $t \geq t^*$ since the exponential function is strictly monotonously increasing, $u(t)$ can be further estimated following

$$\mathrm{e}^t u(t) < u(0) + \int_0^{t^*} \frac{S\mathrm{e}^{\alpha\varphi+s}}{\mathrm{e}^{\varphi v}}\,\mathrm{d}s + \int_{t^*}^t \frac{S\mathrm{e}^{\alpha\varphi+s}}{\mathrm{e}^{\varphi v_0}}\,\mathrm{d}s + \int_0^t \mathrm{e}^s\varphi\,\mathrm{d}s \tag{5.37}$$

$$= u(0) + \int_0^{t^*} \frac{S\mathrm{e}^{\alpha\varphi+s}}{\mathrm{e}^{\varphi v}}\,\mathrm{d}s + S\mathrm{e}^t\mathrm{e}^{\varphi(\alpha-v_0)}(1-\mathrm{e}^{-t+t^*}) + \mathrm{e}^t\varphi(1-\mathrm{e}^{-t}). \tag{5.38}$$

Thus,

$$u(t) < \mathrm{e}^{-t}u(0) + \mathrm{e}^{-t}\underbrace{\int_0^{t^*} \frac{S\mathrm{e}^{\alpha\varphi+s}}{\mathrm{e}^{\varphi v}}\,\mathrm{d}s}_{<\infty} + S\mathrm{e}^{\varphi(\alpha-v_0)}(1-\mathrm{e}^{-t+t^*}) + \varphi(1-\mathrm{e}^{-t}), \tag{5.39}$$

and finally

$$\limsup_{t\to\infty} u(t) < S\mathrm{e}^{\varphi(\alpha-v_0)}(1-\underbrace{\mathrm{e}^{t^*}}_{<\infty}) + \varphi \tag{5.40}$$

$$< S\mathrm{e}^{\varphi(\alpha-v_0)} + \varphi < \infty. \tag{5.41}$$

□

Proposition 3. *Model* (5.1) *contains an equilibrium point which is globally asymptotically stable.*

Proof. In Section 5.1.1 it is proven that the set-point is an equilibrium point independent of the individually derived set-point equations. More specifically, the set-point is a locally asymptotically stable spiral point.
Lemma 3 proves that all trajectories of model (5.1) are constrained in a bounded region of $\mathbb{R}^2_+$ and therefore, according to the Poincaré-Bendixon Theorem, the set-point is globally asymptotically stable since Lemma 2 rules out periodic orbits and graphics. □

5.2 Equilibrium Behavior of the Unified Model of the Thyroid Hormone Regulation

Following the same mathematical procedure as applied in 5.1 it can be proven that the trajectories of the model presented in 4.2 converge to the steady state $(TSH^*, FT4^*)$.

Proposition 4. *Model* (4.28) *contains an equilibrium point which is positive, unique and globally asymptotically stable.*

Proof. The proof of this theorem is given only in outline and can be found in detail in the appendix of [YTH+21].
First, it is shown that the thyroid model (4.28) contains a unique positive state by setting the equations to zero and solving them for the corresponding variable. The property of local asymptotic stability of this equilibrium point is proven using the eigenvalues of the Jacobian matrix. Using Dulac's Criterion (2) and the Poincaré-Bendixon Theorem (3) it is shown that the steady state is also globally stable by rewriting the system and analyze the limes superior and inferior of the corresponding trajectories of both hormones. Therefore it can be deduced that all trajectories of the model converge to this unique equilibrium point. □

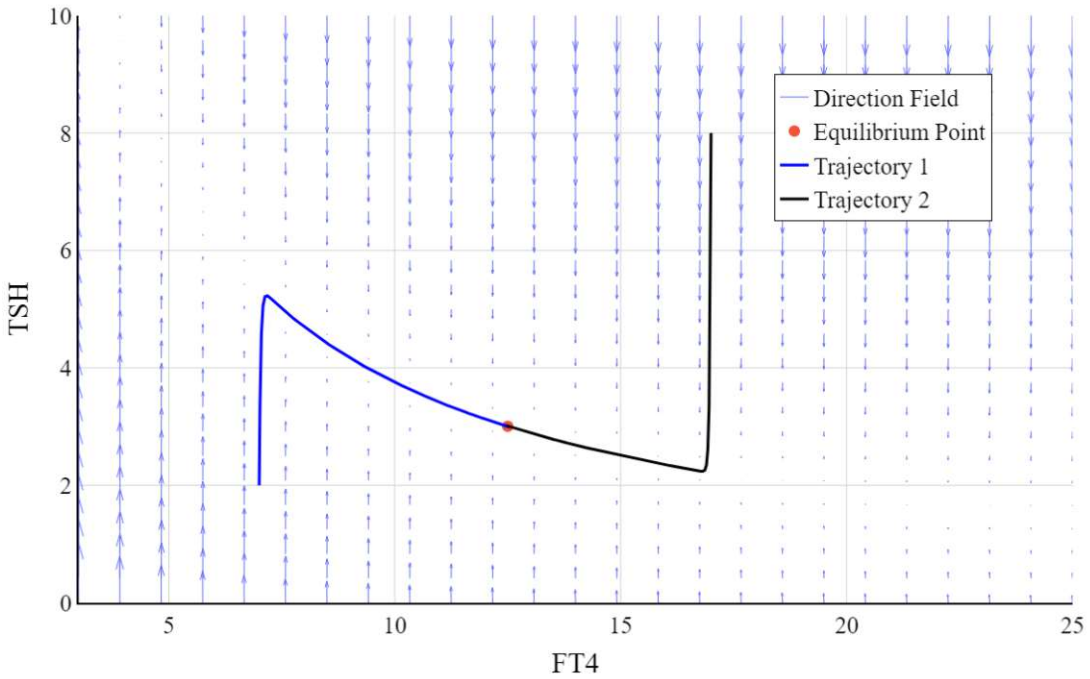

Figure 5.2: Direction field of model (4.28) including two sample trajectories. The equilibrium point is given as $[FT4^*, TSH^*] = [12.5, 3]$. The initial value for trajectory 1 is $[7, 2]$ and for trajectory 2 it is $[17, 8]$. The exemplary parameter set was chosen to be $[p_1, s_1, s_2, d_1, d_2, U, G] = [50, 0.0434, 0.0021, 16.6355, 0.099021, 12.5, 0]$ given in [YTH+21].

The existence of a globally asymptotically stable equilibrium point can also be observed in Fig. 5.2.

The equilibrium was not classified during the theoretical qualitative analysis since the analytic expression does not allow for an explicit determination of the eigenvalues of the Jacobian matrix. The direction field allows the point to be classified as a stable node since the arrows are slightly tilted towards it.
Furthermore, the trajectories converge directly to the equilibrium point if they start on the exponentially shaped zero change line, which is marked by almost unobserved arrows in the direction field. The trajectories converge to the equilibrium point regardless of their initial value, whereby it can be observed that first the TSH value is adjusted until the zero change line is reached, while the FT4 value then controls the convergence to the respective steady state.

6 Data-Based Model Analysis

The models described in the last chapters can now be used to simulate the course of thyroid hormones in the state space and time domain. Based on the patient data presented in section 2.3, the parameter identification is conducted as generally described in section 3.4. The two models analyzed in detail in chapter 4 form the foundation for the simulation. Corresponding details and results of those two models including several approaches will be presented and discussed in the following sections.

6.1 Calibration

To simulate the course of the hormone concentration [TSH] and [FT4], the minimal model of the HPT axis introduced in section 4.1 is combined with the corresponding mathematical analysis presented in chapter 4. There are two approaches focusing on the simulation of the long-term behavior of the HPT complex, which will be described in detail in the following subsections. Both approaches require the parameter identification of two or four parameters, respectively. The bounds used for the calibration are presented in Table 6.1.

Parameter	Bounds
S	$[1000, 1500]$
φ	$[0.2, 0.5]$
A	$[20, 100]$
α	$[0.1, 0.4]$

Table 6.1: Calibrated parameters and corresponding bounds of the minimal model (4.1).

The parameters included in Table 6.1 do not possess a physiological meaning. Thus, the determined bounds are chosen based on previous calibrations conducted in [LG14].
In Fig. 6.1, the resulting distribution of the four parameters of model (4.1) for both state space and direct calibration is presented.
It shows that while each parameter of the state space fit contains at least one outlier, the values obtained from the direct calibration do not. The only parameter including more than one outlier is S, where the outliers show very close values. The parameters φ and A determined by the state space calibration have a significantly lower range compared to the time domain calibration.
The range of the parameter values of S, φ and A resulting from the calibration in the time domain contains the entire range of the same parameters from the state space calibration, except for an outlier of S. In contrast to this observation, the range of the parameter α overlaps in both approaches only at one value, which is an outlier with respect to the state space calibration. The parameter α also shows a similar width of distribution for both

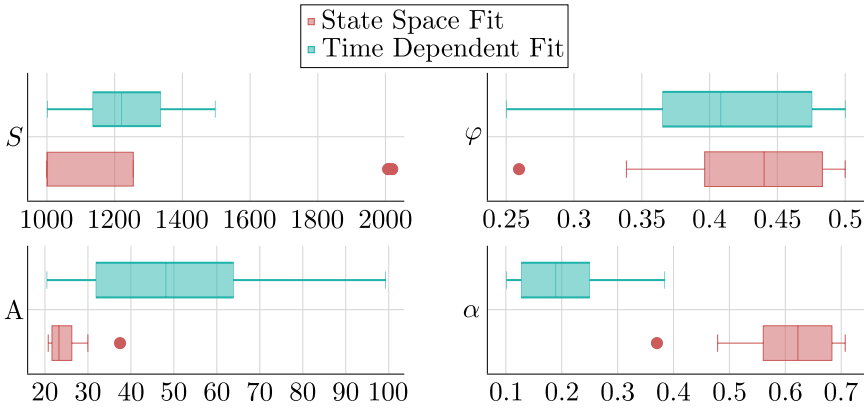

Figure 6.1: Boxplots of the calibrated parameters of model (4.1) for both state space and time domain calibration.

approaches. In general, a broader distribution can be observed for most of the parameters for the calibration in the time domain.

The first modeling approach is based on the calibration of the HP-function in the state space as described in section 4.1.6. This provides a parameter identification of S and φ, which then allows for computing the set-point applying the maximum curvature theory as presented in section 4.1.1. Based on the set-point values of [TSH] and [FT4], the remaining parameters A and α can be determined by using the results of the gain factor analysis developed in section 4.1.3. Thus, the time-dependent course is simulated based on the state space calibration.
The second calibration approach relies on the identification of the course of both hormones and is described in section 4.1.6. The approach is based on an identification of all parameters S, φ, A and α in the time domain with respect to the corresponding course of [TSH] and [FT4]. Based on the identified parameters, the state space curves can also be determined, which provides the possibility to compare the respective hormonal course.

The time-dependent course of both hormones can also be simulated using the unified model of the thyroid hormone regulation presented in section 4.2. The corresponding parameter identification is described in detail in section 4.2.4. The model includes several parameters, four physiologically determined and two requiring parameter identification. Table 6.2 shows the values of the parameters that are taken from the literature.

Parameter	Unit	Value
d_1	day^{-1}	16.6355
d_2	day^{-1}	0.099021
s_1	$\text{pg} \cdot \text{mL}^{-1}$	0.0434
s_2	$\text{mU} \cdot \text{L}^{-1}$	0.0021

Table 6.2: Physiologically determined parameter values of the unified model (4.28) based on the description given in [Pan11].

Table 6.3 contains the remaining parameters that are determined during the parameter identification.

Parameter	Unit	Bounds
p_1	$\mathrm{mU} \cdot \mathrm{L}^{-1} \cdot \mathrm{day}^{-1}$	$[0.001, 1000]$
U	$\mathrm{pg} \cdot \mathrm{mL}^{-1}$	$[7, 18]$

Table 6.3: Calibrated parameters and corresponding bounds of the unified model (4.28).

The boundary interval for U was chosen according to its definition of the set-point value of [FT4], and thus corresponds to the normal range of [FT4] as given in section 2.1. Since p_1 corresponds to the standard release rate of [TSH] from the pituitary gland when [FT4] is at the euthyroid set-point value, the bounds cannot be derived physiologically resulting in a broader interval.
Figure 6.2 shows the distribution of both parameters of the unified model (4.28) resulting from a calibration of the time-dependent hormonal course.

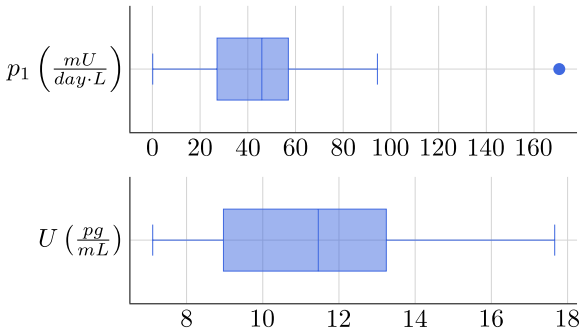

Figure 6.2: Boxplots of the calibrated parameters of the unified model (4.28).

While the parameter U does not contain any outlier, p_1 includes one. It is noticeable that the range of the value of p_1 is very large which is attributable to the corresponding boundary interval. Almost 50 percent of the values of p_1 can be found between almost 0 and 43 $\mathrm{mU} \cdot \mathrm{L}^{-1} \cdot \mathrm{day}^{-1}$, the remaining percentage is between 43 and about 98 $\mathrm{mU} \cdot \mathrm{L}^{-1} \cdot \mathrm{day}^{-1}$. The values of parameter U extend over almost the entire possible range determined by the boundary interval.

Figure 6.3 shows an exemplary course of the value of the corresponding objective function with respect to the different calibrations and steps of the optimizer differential evolution, described in detail in section 3.4.
In the course of the state space calibration of the minimal model, the optimal parameter values of the HP-function are determined, as described in detail in section 4.1.6. Therefore, the value of the objective function of this approach does not correspond to the NMSE with respect to the time domain as for the other curves. Thus, its NMSE is lower since only the HP-curve is fitted to the corresponding data points.
In both approaches of the minimal model, the error hardly decreases during the optimization, which leads to the conclusion that the initial parameter set has already resulted in an

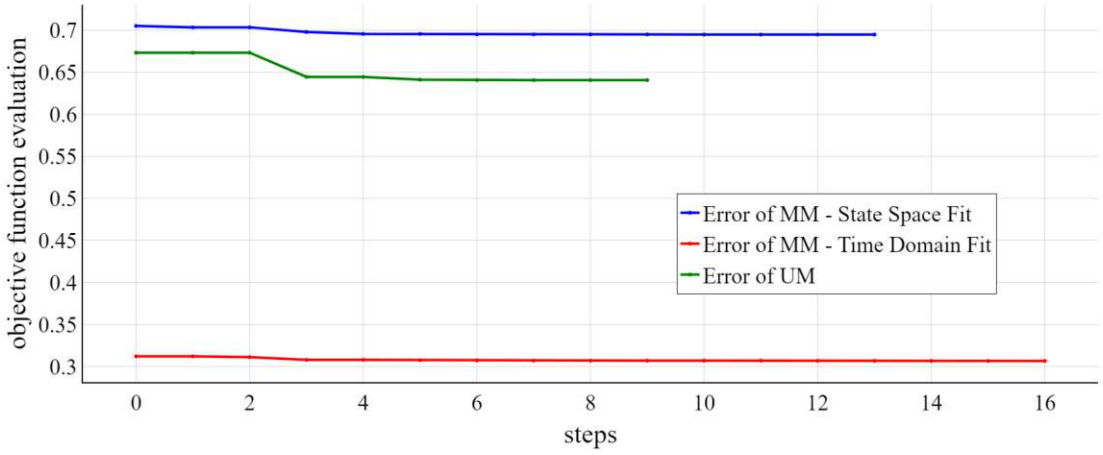

Figure 6.3: Exemplary course of the objective function during the optimizing steps of differential evolution with respect to both models and corresponding approaches.

adequate fit. The NMSE curve of the unified model shows a decrease between the second and third optimization step before it remains almost constant. In addition, the optimal parameters of the unified model were determined with a smaller number of optimization steps, while almost twice as many steps were required to fit the minimum model in the time domain.
It can be concluded that the solution curves obtained by the initial set of parameters of the calibration almost fulfill the requirements given by the differential evolution algorithm.

6.2 Simulation Results

After calibrating the models, the course of both [TSH] and [FT4] can be simulated. Three exemplary patients are selected to describe the behavior and the differences of the presented models.

Patient 11 suffers from autoimmunthyreoiditis and is 60 years old at the time of the first measurement. In total, eight measurements are included in the data set and the corresponding time span extends over 74 weeks. During this time, the patient was prescribed a certain dose of thiamazole before receiving T4 instead. The maximum TSH and minimum FT4 concentrations can be observed during the administration of thiamazole.
Figure 6.4 shows the calibration results in state space including the corresponding data points of patient 11.
The data set of patient 11 includes measurements which show very different magnitudes of the hormones, as shown in Fig. 6.4. In correspondence with the physiological behavior presented in 2.1, the maximum value of [TSH] is associated with the minimum [FT4] concentration. The highest [FT4] measurements also correspond to the lowest [TSH].

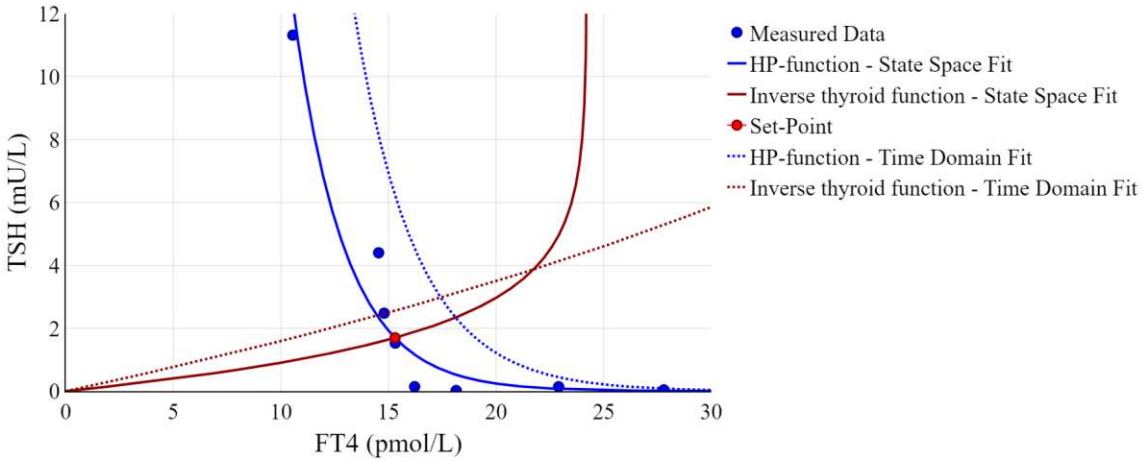

Figure 6.4: Patient 11 - Simulation of the course of [TSH] and [FT4] in state space resulting from both calibration approaches of the minimal model (4.1) including the calculated set-point and measured data.

Figure 6.4 additionally shows that the HP-function (4.3), calibrated using the state space fit described in section 4.1.6, represents the data points of patient 11. Especially the data points containing the lowest and highest [FT4] concentrations are located almost directly on the curve. The set-point is the point of maximum curvature of the HP-function according to section 4.1.1 and can be found very close to one of the measurement points. Additionally, it represents the points of intersection between the inverse thyroid function (4.18) and the HP-function (4.3).
The HP-function and thyroid function, determined using the parameter identification in the time domain described in section 4.1.6, are also included in Fig. 6.4. Compared to the state space fit, the blue dotted HP curve is shifted to the left and intersects only the measurement point with the maximum [FT4] concentration. The red dotted thyroid curve shows a flatter course and intersects the corresponding HP curve at a point of higher [TSH] and [FT4] concentration than the set-point.
The blue HP curve indicates that a low [FT4] value leads to a high release of [TSH] by the HP complex and vice versa due to the negative feedback loop. The red inverse thyroid curve on the other hand reflects a high secretion of [FT4] by the thyroid complex in response to a high [TSH] concentration according to the stimulation by the HP complex. Independent of the approach, both functions can be considered as response curves.
Figure 6.5 shows the corresponding time-dependent course of patient 11 of both approaches. Additionally, the resulting curves of the unified model described in section 4.2 are included. As shown in Fig. 6.5, the state space calibration yields a time-dependent course of [TSH] and [FT4] representing a dynamic behavior during the first five weeks prior to reaching an equilibrium. It can be seen that the corresponding [FT4] curve decreases, increases and decreases again before leveling off at the equilibrium. On the other hand, the [TSH] curve increases in response to the decreasing [FT4] concentration before minimally decreasing

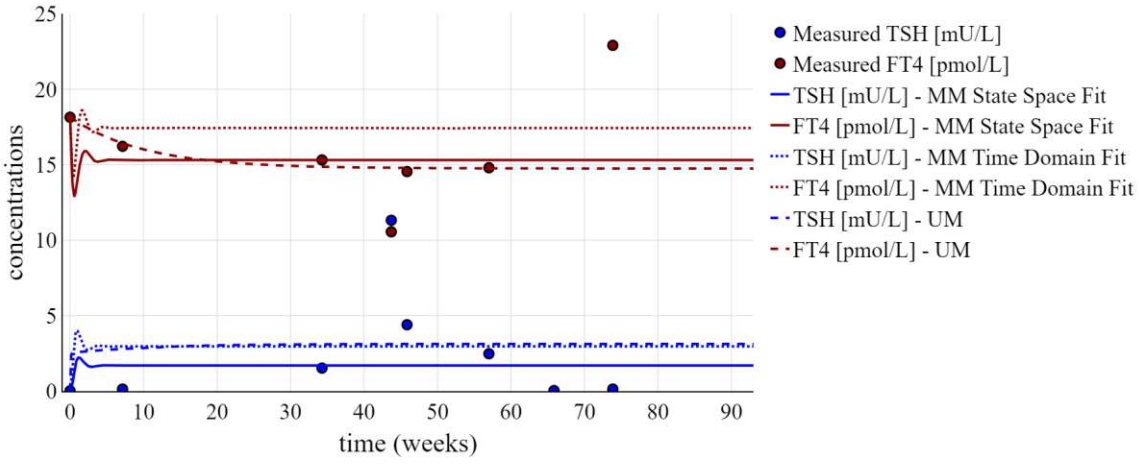

Figure 6.5: Patient 11 - Simulation of the time-dependent course of [TSH] and [FT4] resulting from calibration of the unified model (4.28) and both calibration approaches of the minimal model (4.1) including measured data.

again and reaching the equilibrium. Therefore, the represented dynamics accurately reflect the physiological behavior of the HPT complex. Both hormonal curves intersect with one data point of a measurement point pair while they have already reached the equilibrium. The dotted curves resulting from the calibration in the time domain show a similar dynamic behavior during the first six weeks before leveling of at an equilibrium. The course of the [FT4] curve starts with a short steep decrease in concentration before rapidly increasing resulting in a [FT4] value larger than the starting point. The equilibrium is reached after a smaller decrease followed by a minor increase in concentration. The starting dynamics of the [TSH] curve can be found in a shorter time interval than the corresponding [FT4] curve. In response to the rapid decrease of [FT4], [TSH] increases at first before decreasing and leveling off at the equilibrium in line with the underlying physiological dynamics. In contrast to the state space fit, the time domain fitted curves do not intersect any measurement points. Additionally, both curves result in an equilibrium of higher hormonal concentration compared to the first approach.
The resulting hormonal courses of the calibration of the unified model (4.28), described in section 4.2.4, are also included in Fig. 6.5. Both hormonal concentrations reach an equilibrium after approximately 30 weeks. This equilibrium is close to the continuous curve for [FT4] and almost the same as the curve for [TSH]. During the first 30 weeks, a continuous decrease in the concentration of [FT4] can be observed. During the same time span, the [TSH] concentration increases until the equilibrium is reached.
The corresponding determined parameters and the resulting value of the objective function for both models are presented in Table 6.4.
It can be observed that the two approaches to calibrate the minimal model lead to differences in all four parameters. The smaller value of the parameter φ for the time domain calibration approach results in the right-shifted HP curve shown in Fig. 6.4 due to a slower

Minimal Model	$[FT4]_{sp}$	$[TSH]_{sp}$	S	φ	A	α	NMSE
State Space Fit	15.31	1.7	1000.81	0.42	24.22	0.59	2.97
Time Domain Fit			1286.21	0.35	66.94	0.1	2.6
Unified Model	U	p_1					NMSE
	14.75	52.04					2.32

Table 6.4: Patient 11 - Numerical results including parameters, set-point and NMSE.

decrease. The parameter S is found in the same order of magnitude in both approaches. The smaller value of α results in a flatter curve of the inverse thyroid function while the right-shift is caused by the increased parameter A.
Both models include a set-point value for [FT4], listed in Table 6.4 as $[FT4]_{sp}$ and U, respectively. The set-point value of the minimal model, $[FT4]_{sp}$, is slightly larger than the respective value of U for the unified model, but both can be found close to 15 pmol/L. These values represent the equilibrium states reached by the corresponding [FT4] curves shown in Fig. 6.5.
The lowest NMSE for patient 11 is found for the unified model with a magnitude of 2.32. The maximum of 2.97 is reached when identifying the parameters based on the state space calibration of the minimal model. Due to two pairs of measurements that deviate significantly from the other values, the minimum NMSE is still high compared to the results of other patients, who are presented in the following.

Patient 18 was diagnosed with Hashimoto autoimmune thyreoiditis and is 23 years old during the time of the data acquisition. The data set includes five measurements collected over a time period of 37 weeks. Patient 18 received thiamazole upon the first visit and T4 upon the last visit. No thyroid medication was prescribed between these two visits. The calibration results for patient 18 are presented in the following.
Figure 6.6 shows the course of [TSH] and [FT4] in state space including the corresponding data points.
The HP-function of the state space fit intersects with the point of maximum [TSH] and decreases almost centered between the remaining data points. It intersects the corresponding inverse thyroid function at the set-point, which lies outside the data point cloud and is determined by a lower [TSH] and higher [FT4] compared to the measurements. The HP-functions of the two calibration methods are almost identical. In contrast, the inverse thyroid function of the time domain fit shows a steeper increase than the resulting curve of the state space fit. It intersects the HP-function at a point with a higher [TSH] and lower [FT4] compared to the set-point. In addition, this point of intersection is in the middle of the data point cloud, unlike the set-point.
The corresponding time-dependent hormonal course of both approaches is shown in Fig. 6.7. The time-dependent course of both [TSH] and [FT4] of the state space fit shows a dynamic behavior during the first seven weeks before reaching an equilibrium. The high initial value of [TSH] results in an increasing [FT4] at the beginning. As [TSH] decreases, [FT4] shows the same behavior after a certain delay. Both hormones rise and fall slightly before leveling off at the equilibrium.

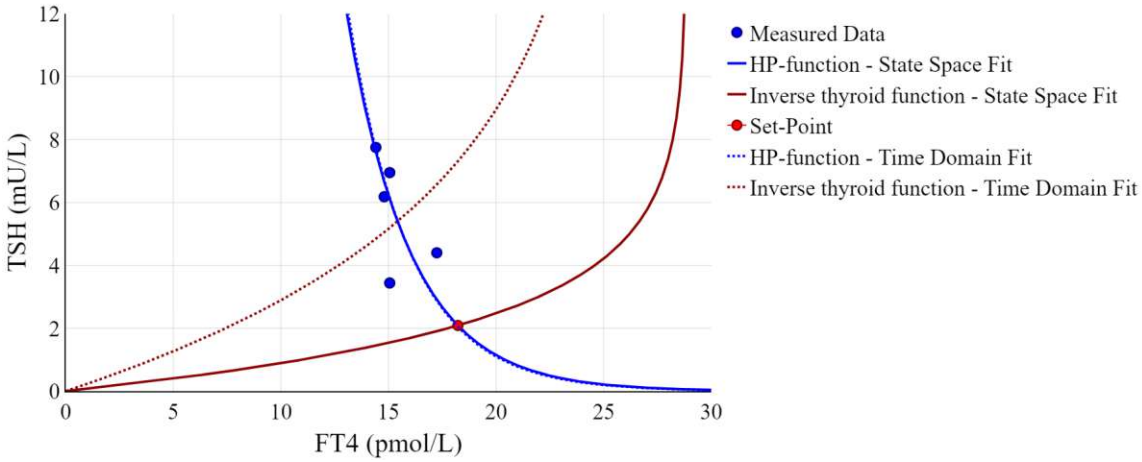

Figure 6.6: Patient 18 - Simulation of the course of [TSH] and [FT4] in state space resulting from both calibration approaches of the minimal model (4.1) including the calculated set-point and measured data.

The [FT4] and [TSH] state space calibration curves are located above and below the corresponding data points, respectively.
Compared to the state space fit, the dynamic behavior of the curves resulting from the time domain calibration is found in a shorter time interval. Additionally, no slope of the same magnitude can be observed for either of the two curves during this time interval. The steady state of both curves lies within the measuring points for [TSH] as well as [FT4].

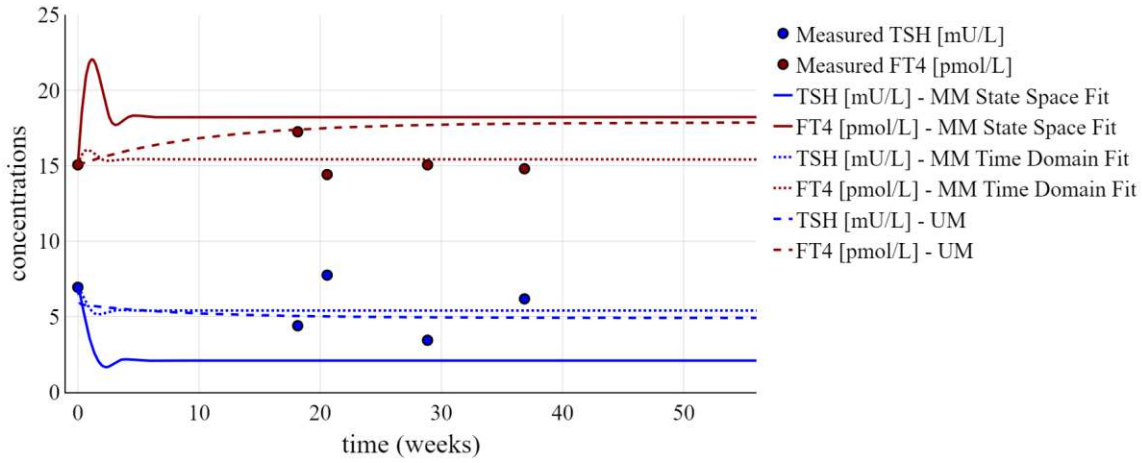

Figure 6.7: Patient 18 - Simulation of the time-dependent course of [TSH] and [FT4] resulting from calibration of the unified model (4.28) and both calibration approaches of the minimal model (4.1) including measured data.

The course of [FT4] determined by the unified model increases during the first 30 weeks and intersects with the second measurement point before reaching an equilibrium. This equilibrium point is found close to the steady state of the [FT4] curve of the state space calibration of the minimal model. In contrast, the [TSH] curve of the unified model decreases during the same time, but levels off at an equilibrium close to the [TSH] course determined by the time domain fit of the minimal model.
The corresponding parameters including the NMSE are presented in Table 6.5.

Minimal Model	$[FT4]_{sp}$	$[TSH]_{sp}$	S	φ	A	α	NMSE
State Space Fit	18.23	2.09	1000.95	0.34	28.83	0.48	4.99
Time Domain Fit			1150.68	0.35	25.37	0.17	0.85
Unified Model	U	p_1					NMSE
	17.86	81.75					0.88

Table 6.5: Patient 18 - Numerical results including parameters, set-point and NMSE.

The parameters S and φ do not differ much for both calibration approaches of the minimal model resulting in the almost identical curves of the HP-function in Fig. 6.6. The value of α is smaller for the time domain fit resulting in a steeper increase of the corresponding inverse thyroid function although A does not differ much for both approaches.
The NMSE of the state space fit is almost six times as high as for the time domain calibration. This result is also shown in Fig. 6.7 as the corresponding curves of both hormones lie outside the respective data points. The set-point coordinate of [FT4] of the minimal and the unified model to not differ much, which corresponds to the close equilibrium of the [FT4] curves shown in Fig. 6.7. The lowest error is achieved for the calibration of the minimal model in the time domain, closely followed by the unified model.

Patient 65 suffers from latent hypothyroidism with serological evidence of autoimmune thyreoiditis and is 30 years old at the time of the first measurement. At this time she is also in the ninth week of pregnancy. The corresponding data set contains five measurements in total, collected over a time period of 38 weeks. The prescribed dose of T4 remains constant over the period of available measurements. No other medication use is recorded. In her diagnosis it was additionally noted that she is sufficiently thyroxine-treated.
The state space and time dependent hormonal course resulting from the different approaches of parameter identification are presented below.
Figure 6.8 shows the course of [TSH] and [FT4] for patient 65 in the state space including the corresponding data points. Almost all of the measurements can be found in a similar range. Only one point, which corresponds to the first measurement available in the data set of patient 65, deviates from the others. Both state space and time dependent calibration result in a very similar curve for HP-function represented in blue. It intersects with the red inverse thyroid function at the set-point that can be found very close to the majority of the data points. In contrast to the HP-function, the inverse thyroid function differs for both approaches. A steeper increase of the curve can be observed for the state space calibration than for the time domain fit.

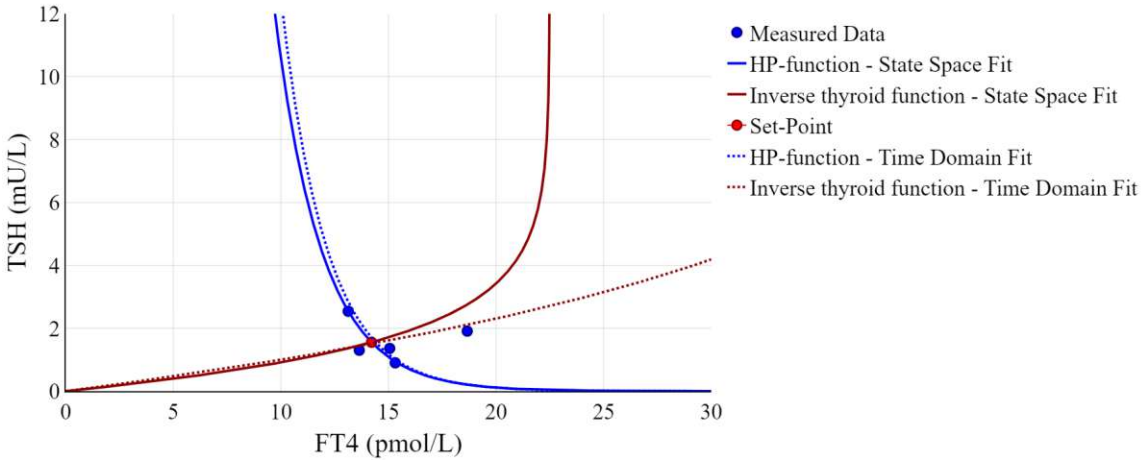

Figure 6.8: Patient 65 - Simulation of the course of [TSH] and [FT4] in state space resulting from both calibration approaches of the minimal model (4.1) including the calculated set-point and measured data.

The corresponding time-dependent hormonal course and determined parameters are presented in Fig. 6.9.
The hormonal courses for the minimal model for both approaches show a dynamic behavior during the first eight weeks which corresponds to the time until the second measurement. For both state space and time domain fit, a decrease in concentration followed by an increase can be observed for [TSH] and [FT4]. After a small decrease, the equilibrium state is reached.

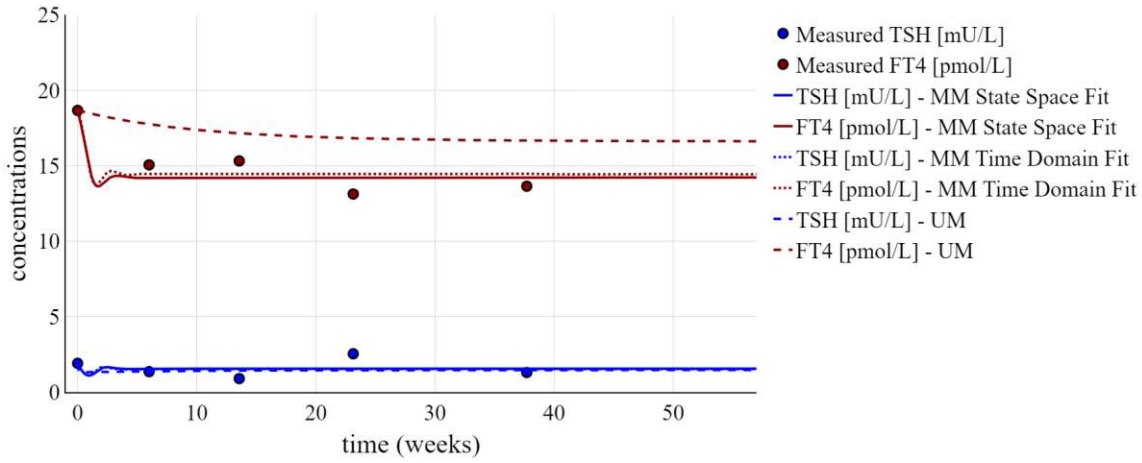

Figure 6.9: Patient 65 - Simulation of the time-dependent course of [TSH] and [FT4] resulting from calibration of the unified model (4.28) and both calibration approaches of the minimal model (4.1) including measured data.

The curves for [TSH] and [FT4] for state space and time domain fit are very close to each other both during the time interval of the dynamic behavior and when equilibrium is reached. The equilibrium can be found close to the average of the data points excluding the starting value.
For [TSH] this equilibrium is also very close to the corresponding curve of the unified model. The [TSH] curve resulting from this model shows a steep increased during a very small time interval at the beginning before leveling off at the equilibrium. In contrast to this behavior, the corresponding [FT4] curve differs significantly from the results of the minimal model. The whole course of [FT4] can be found in an interval of larger concentration values including the final equilibrium. It takes about 30 weeks to reach an equilibrium. During this time the [FT4] concentration decreases.
The corresponding parameters including the normalized mean squared error of all approaches are presented in Table 6.6.

Minimal Model	$[FT4]_{sp}$	$[TSH]_{sp}$	S	φ	A	α	NMSE
State Space Fit	14.21	1.55	1000.53	0.45	22.49	0.64	0.313
Time Domain Fit			1419.06	0.47	48.17	0.23	0.305
Unified Model	U	p_1					NMSE
	16.62	24.51					0.64

Table 6.6: Patient 65 - Numerical results including parameters, set-point and NMSE.

As shown in Table 6.6, the parameter S is found in the same order of magnitude for both state space and time domain fit. In contrast, the parameter φ only differs minimally resulting the very close curves for the HP-function shown in Fig. 6.8. The smaller value of A and larger value of α for the state space fit results in a steeper course of the inverse thyroid function. The set-point values of the unified and the minimal model differ by about 2.4 pmol/L and correspond to the equilibrium reached by the corresponding [FT4] curves in Fig. 6.9.
The minimum NMSE resulting from the final evaluation of the objective function can be found with the time domain fit of the minimal model and does not differ significantly from the state space calibration approach. The simulation based on the unified model results in a NMSE twice as high as both approaches of the minimal model.

In Table 6.7, the resulting NMSE of each calibration approach with respect to the individual patient data set is presented. The mean and standard deviation of the NMSE for each approach is included for an overall comparison.
The maximum NMSE of the state space calibration of the minimal model is found for patient 66. This patient is also associated with the maximum NMSE of the unified model. Patient 11 has the highest NMSE of the time domain fit of the minimal model, which is significantly lower than the maximum value of the other two approaches.
The minimum NMSE of the state space fit is achieved for patient 65, whose calibration results are presented in detail above. For this patient also the other two approaches result in a low NMSE. In contrast, while the lowest NMSE of the time domain fit is found for patient 60, the NMSE of the other two approaches is significantly larger.

Patient	MM - State Space	MM - Time Domain	UM
2	1.03	0.76	1.05
3	3.99	0.80	3.65
5	1.05	0.68	0.83
11	2.97	2.60	2.32
12	1.08	0.38	0.35
13	3.17	0.69	0.86
18	4.99	0.85	0.88
22	2.76	1.21	1.39
33	1.75	0.54	1.32
35	2.40	1.15	1.18
37	0.96	0.14	3.40
53	0.80	0.70	1.42
54	1.11	0.78	1.13
55	0.91	0.69	0.83
56	1.19	1.13	1.25
57	0.92	0.47	0.63
59	0.81	0.32	0.90
60	3.42	0.13	3.79
61	2.35	2.03	1.67
62	0.42	0.37	0.73
63	1.49	1.07	1.12
64	0.56	0.41	1.03
65	0.31	0.31	0.64
66	5.28	1.22	5.65
71	1.65	1.05	0.86
mean	1.90	0.82	1.53
std	1.37	0.55	1.16

Table 6.7: Normalized mean squared error of each calibration for all of the patients included in the base data set. The mean and standard deviation of the results are added for each model and calibration approach, respectively.

Patient 12 has the minimum NMSE of the unified model that is close to the NMSE of the time domain calibration of the minimal model. In contrast, the NMSE of the state space calibration of this patient is about three times as high.
The time domain fit of the minimal model results in the lowest mean NMSE and standard deviation over all included patients. In comparison, the mean NMSE and standard deviation of the calibration of the unified model is about twice as high. The largest mean NMSE and standard deviation are found for the state space fit of the unified model.

7 Discussion

In this work two mathematical models describing the HPT complex using a system of differential equations were analyzed in terms of individual set-point, stability behavior and ability to reflect patient data in the course of a simulation. Mathematical modeling of the HPT complex provides insight into the mutual influence of the individual compartments, which is not yet fully understood, especially with regard to the patient-specific hormonal equilibrium.

In the publications [LG14] and [Goe21], the so-called minimal model is presented including two approaches to theoretically derive the set-point. The maximum curvature theory describes the set-point as the point around which the pituitary is most sensitive to any changes in concentration of [FT4]. It is thus determined as the point where the derivative of the curvature of the HP-function, the equilibrium function of the differential equation of [TSH] of this model, is zero. Since the set-point is defined as the hormonal equilibrium and the secretion of thyroid hormones is based on the mutual influence of the compartments, the thyroid gland is analogously most sensitive to changes in [TSH] around this point. To analyze the general applicability of the maximum curvature theory, it is therefore applied to the thyroid function, the equilibrium function of the differential equation of [FT4] of this model. Both applications result in an explicit expression of the set-point of both [TSH] and [FT4].

The gain factor analysis is the second approach to derive an explicit expression for the set-point. It is defined as the point at which the HPT complex, or more precisely the loop gain when represented as a negative feedback closed-loop system, operates optimally.
These two mathematical theories result in three equations for the set-point coordinate of [TSH] and [FT4], respectively. Additionally, the maximum curvature theory applied to the thyroid function and the gain factor analysis describe both set-points in dependence on the same two parameters. This leads to a two-dimensional system of equations with two unknowns and seemingly provides the possibility to describe those parameters independently of the set-point. The system is not explicitly solvable, but the expressions are non-contradictory subject to a condition on the parameters. Thus, in this work, it is shown that the maximum curvature theory is not only applicable to the function in whose context it was published, but also leads to an explicit expression for the set-point that does not contradict the previously published results when applied to the thyroid function.

Another model of the time-dependent dynamics of the HPT complex is presented in [YTH+21]. In line with the minimal model, this so-called unified model consists of a system of two differential equations for [TSH] and [FT4] and includes the set-point as individual hormonal equilibrium. In contrast to the minimal model, the set-point is not derived by

mathematical approaches but explicitly included as parameters. Thus, in this work it is used as a comparative model. The maximum curvature theory and the gain factor analysis, originally introduced for the minimal model, are applied to the unified mode to fulfill the aim of this work of analyzing their general validity. While the maximum curvature theory applied to both corresponding equilibrium functions of [TSH] and [FT4] results in an explicit expression for the set-point, the computation of the maximum loop gain determines it as the zero point, which is contradictory to its definition of the patient-specific hormonal equilibrium. Nevertheless, in the course of the gain factor analysis the unified model is represented as a closed loop system by deriving the gain factors of the compartments representing the HP complex and the thyroid. It is shown that the maximum curvature theory and the gain factor analysis, although originally introduced for another model, are applicable in the context of the unified model. The maximum curvature theory even results in explicit terms for the set-point in line with the results presented for the minimal model.

Both models describe the HPT complex based on a system of differential equations. Until this point, the set-point is described using mathematical theories or by explicitly including it in the model as parameters. The representation as systems of differential equations provides the possibility to contextualize the set-point with the stability behavior of the system and theoretical equilibrium points. This allows for a conclusion about the relationship between theoretical and endogenous hormonal equilibrium. Thus, a qualitative analysis is conducted for both models. The equilibrium point of the minimal model cannot be explicitly determined due to coupled functions, but it can be shown that the previously derived set-point equations represent locally stable equilibrium points. For this analysis, the system is linearized and by the use of properties of the respective Jacobian matrix eigenvalues, the local stability behavior is determined. The global asymptotic stability is shown by proving that the Dulac-Bendixon-Criterion and the Poincaré-Bendixon-Theorem apply to the minimal model. The combination of both implications allows for the conclusion that all trajectories of the model tend to the set-point with increasing time, which is also shown in the corresponding phase plot. As a result, the set-point, derived by mathematical theories, can be classified as a globally asymptotically stable point of the corresponding system.

In [YTH+21], the existence of a unique equilibrium point, which is globally asymptotically stable, is already shown in the corresponding publication. Thus, a short summary of the proof, which is based on the same theories applied to the minimal model, is given. The qualitative analysis is motivated by the corresponding phase plot, which shows that the value of [TSH] of trajectories is changed very fast during the first time steps, while [FT4] is nearly constant. Only after the zero change line is reached, the trajectory significantly converges towards the equilibrium point. This result verifies the stability behavior reflecting the underlying physiology, since [TSH] has a much smaller half-time than [FT4].

The theoretical results are contextualized with patient data collected at the Vienna General Hospital during a study conducted by the Medical University of Vienna (MUW) in the course of a simulation of the models. Two approaches are pursued to simulate the time-dependent course using the minimal model. The state space fit is based on a parameter identification of the HP-function in the state space and a subsequent calculation of the

remaining parameters based on the set-point equations. In the course of the time domain fit, all parameters are identified with respect to the time domain. The resulting curves in both state space and time domain are presented for three exemplary patients.

In the state space plots, it is shown that the HP and the inverse thyroid function, considered as response functions, accurately represent the physiological dynamics. In line with the stimulating effect of [TSH] on the thyroid, a high [TSH] leads to a high release of [FT4], which is represented by the inverse thyroid function. In correspondence to the negative feedback loop, a high value of [FT4] leads to a low secretion of [TSH] by the HP complex. This behavior can be observed on the curve of the HP-function.
The HP-function resulting from the state space fit accurately represents the data points of all exemplary patients. In contrast, the HP-function determined by the time domain calibration does not fit all data, but can be very similar to the corresponding function of the state space fit. Even if both HP-functions are nearly equal, a different course of the resulting curves of inverse thyroid function can be observed. Independent of the calibration approach, the set-point corresponds to the point of intersection of both HP and thyroid function. The location of the set-point with respect to the patients measurements differs. For some patients, it is found close to the center of the data point cloud. For others, it is not placed within the point cloud, because the measurements do not lie around the knee region of the HP-function. The set-point coordinates of both approaches are not equal. In most cases the value of the respective [TSH] value of the time domain fit is larger compared to the state space fit.

In the time domain, the resulting time-dependent solution curves of both models and corresponding approaches are computed. The course of both [TSH] and [FT4] determined by the minimal model show a dynamic behavior during the first 5 weeks before reaching an equilibrium. This dynamic accurately represents the physiological mutual influence of both hormones. If the [FT4] curve decreases, the [TSH] curve increases after a small time delay and vice versa until the equilibrium is reached. The duration of the dynamic behavior of [FT4] corresponds to its endogenous decomposition. According to [AÖO$^+$18], the half-life of [FT4] is around 7 days and the it takes about 5 half-times until [FT4] reaches its steady state. This corresponds to the findings presented in [AER$^+$21] stating that an [FT4] equilibrium can be observed during 4 to 6 weeks after medication intake. For this reasons, blood samples of patients suffering from thyroid diseases are drawn after a time span of about 5 weeks to determine the accurate medication dosage. The equilibrium of the time-dependent curves for [TSH] and [FT4] corresponds to the set-point coordinates. In addition to the stability analysis discussed above, it is now not only theoretically shown, that the set-point is globally asymptotically stable. The simulated time-dependent curves level off at the set-point and do not deviate from it with increasing time, which verifies the theoretical results numerically. According to the sensitivity analysis, the sensitivity of set-point of [FT4] is dominated by only one parameter, while the [TSH] component is sensitive to three parameters. The set-point of [TSH] is most sensitive to a parameter that is not included in the explicitly derived set-point equations used.
Similar to the minimal model, the solution curves of the unified model show a dynamic behavior during the first 30 weeks after reaching an equilibrium. Usually, a shorter dynamic

can be observed for [TSH]. This corresponds to the respective phase plot showing that the value of [TSH] is adjusted prior to [FT4]. Additionally, this behavior is in line with the endogenous decomposition of both hormones since the half-time of [TSH] is about 65 minutes and therefore much shorter compared to [FT4] explaining the faster convergence to the steady state. The equilibrium point is only sensitive to the corresponding parameter determining the set-point state of the respective hormone.

In general, the time domain fit of the minimal model results in the lowest normalized mean squared error for the time-dependent hormonal course with respect to the whole data set used for calibration. The respective state space calibration leads to the largest overall error but shows a good fit of the HP-function to patient data in the state space. It has to be considered that the main purpose of this model is the theoretical description of the set-point and the representation of patient data in the state space. The set-point of the state space fit is found in a physiologically healthy hormonal range and the time-dependent description provides the possibility to contextualize it with the equilibrium behavior. The advantage of the time-dependent fit is that no additional calculations are needed to determine all parameters while it still results in the lowest error with respect to the time-dependent course.

Although none of the models or approaches really reflects the dynamics and data in the time domain, the dynamic behavior of the trajectories until the equilibrium is reached corresponds to the endogenous regulation of both hormones. Additionally, it is shown theoretically and quantitatively that the set-point corresponds to the equilibrium in time domain which is always reached after a certain time span. It can therefore be concluded, that the models suit the purpose of describing the hormonal course when focusing on a physiological individual hormonal equilibrium.

There are several possibilities to further develop the models based on the findings of this work. The main objective during the medical treatment of patients suffering from hypothyroidism is to determine the accurate drug dosage for [TSH] and [FT4] to be in their individual equilibrium. Thus, the medication intake could be included as a model input to analyze its influence on the set-point. Since the models describe the time-dependent hormonal course among others, the time span between medical appointments and the corresponding adjustment of the drug dosage can also be included in the analysis. This approach would contribute to decreasing the number of medical appointments needed to define the accurate individual drug dosage. Additionally, the models described in this work can be used in the future to predict a patients HPT behavior. Using the calibrated model parameters and setting them in context with patient specific data, such as age, sex and medical history, the computation of the patients hormonal equilibrium and the respective optimal medication will be possible.
In conclusion, the overall goal is a valid predication of the patient specific equilibrium, which is verified numerically and theoretically as the set-point in the course of this work, to finally conclude the optimal medication.

List of Figures

List of Tables

Bibliography

[AER+21] Alessandro Antonelli, Giusy Elia, Francesca Ragusa, Sabrina Rosaria Paparo, Gabriella Cavallini, Salvatore Benvenga, Silvia Martina Ferrari, and Poupak Fallahi. The stability of tsh, and thyroid hormones, in patients treated with tablet, or liquid levo-thyroxine. *Frontiers in Endocrinology*, 12, March 2021.

[AM08] K.J. Aström and Richard Murray. Feedback systems: An introduction for scientists and engineers. *Feedback Systems: An Introduction for Scientists and Engineers*, January 2008.

[AÖO+18] Hale Aral, Ömer Faruk Özer, Hatice Onur, Ahmet Mete Çilingirtürk, İlker Tolga Özgen, and Mevlude Ayyıldız. Pediatric reference intervals of free thyroxine and thyroid stimulating hormone in three different hospitals. *Turkish Journal of Biochemistry*, 43(5):530–539, January 2018.

[BA19] Louis G. Birta and Gilbert Arbez. *Modelling and Simulation - Exploring Dynamic System Behaviour*. Simulation Foundations, Methods and Applications. Springer International Publishing, 3rd edition, 2019.

[BBG+21] Hanns-Wolf Baenkler, Robert Bals, Hartmut Goldschmidt, Johannes-Martin Hahn, Martin Hinterseer, Andreas Knez, Matthias Möhlig, Andreas F. H. Pfeiffer, Johannes Schäfer, Hartmut H.-J. Schmidt, Frederik Seiler, Joachim Spranger, Reinhard E. Voll, Mathias Witzens-Harig, and Walter Zidek. *Kurzlehrbuch Innere Medizin*, volume 4. Georg Thieme Verlag KG, 2021.

[CS15] Daniela Calvetti and Erkki Somersalo. *Parameter Identification*, pages 1134–1137. Springer Berlin Heidelberg, Berlin, Heidelberg, 2015.

[CTZFG+21] Manu Centeno-Telleria, Ekaitz Zulueta, Unai Fernandez-Gamiz, Daniel Teso-Fz-Betoño, and Adrián Teso-Fz-Betoño. Differential evolution optimal parameters tuning with artificial neural network. *Mathematics*, 9(4), February 2021.

[Des91] Stefan Silbernagl; Agamemnon Despopoulos. *Taschenatlas der Physiologie*, volume 4. Georg Thieme Verlag, 1991.

[DTPM04] J. W. Dietrich, A. Tesche, C. R. Pickardt, and U. Mitzdorf. Thyrotropic feedback control: Evidence for an additional ultrashort feedback loop fromfractal analysis. *Cybernetics and Systems: An International Journal*, 35(4):315–331, June 2004.

[ESD08] Marisa Eisenberg, Mary Samuels, and Joseph J. DiStefano. Extensions, validation, and clinical applications of a feedback control system simulator of the hypothalamo-pituitary-thyroid axis. *Thyroid*, 18(10):1071–1085, October 2008.

[Fra13] Steven A Frank. Input-output relations in biological systems: measurement, information and the hill equation. *Biology Direct*, 8(31), December 2013.

[GLS+14] Simon Goede, Melvin Leow, Jan Smit, Harald Klein, and Johannes W. Dietrich. Hypothalamus-pituitary-thyroid feedback control: Implications of mathematical modeling and consequences for thyrotropin (tsh) and free thyroxine (ft4) reference ranges. *Bulletin of Mathematical Biology*, May 2014.

[Goe21] Simon Goede. General review on mathematical hpt modeling general review on mathematical modeling in the hypothalamus pituitary thyroid system, December 2021.

[HD19] Robert Haller-Dintelmann. Analysis III – Gewöhnliche Differentialgleichungen. Technische Universität Darmstadt/ Fachbereich Mathematik, February 2019.

[Heu91] Harro Heuser. *Gewöhnliche Differentialgleichungen*, volume 5 of *Mathematische Leitfäden*. Vieweg+Teubner Verlag Wiesbaden, 2 edition, October 1991.

[Hic95] Christian Hick. *Physiologie: Kurzlehrbuch zum Gegenstandskatalog mit Einarbeitung der wichtigen Prüfungsfakten*, volume 1. Jungjohann Verlag, August 1995.

[LG14] Melvin Leow and Simon Goede. The homeostatic set point of the hypothalamus-pituitary-thyroid axis - maximum curvature theory for personalized euthyroid targets. *Theoretical biology and medical modelling*, 11, August 2014.

[LLXL94] Yiwei Liu, Bingzheng Liu, Jiangli Xie, and Y.X. Liu. A new mathematical model of hypothalamo-pituitary-thyroid axis. *Mathematical and Computer Modelling*, 19(9):81–90, 1994.

[Mar15] Maia Martcheva. *An Introduction to Mathematical Epidemiology*. Springer Publishing Company, Incorporated, 1st edition, 2015.

[MM10] Luiz G.A. Martins and Luiz H.A. Monteiro. A model of intelligent controller for hypothyroidism treatment. In *2010 10th IEEE International Conference on Computer and Information Technology*, pages 472–479, 2010.

[MPGGG14] Ane Garmendia Madariaga, Silvia Santos Palacios, Francisco Guillén-Grima, and Juan C. Galofré. The incidence and prevalence of thyroid dysfunction in europe: A meta-analysis. *The Journal of Clinical Endocrinology and Metabolism*, 99(3):923–931, March 2014.

[NEB11] Jiri Nossent, Pieter Elsen, and Willy Bauwens. Sobol' sensitivity analysis of a complex environmental model. *Environmental Modelling & Software*, 26(12):1515–1525, December 2011.

[Pan11] Balamurugan Pandiyan. Mathematical modeling and dynamical analysis of the operation of the hypothalamus - pituitary - thyroid (hpt) axis in autoimmune (hashimoto's) thyroiditis. e-Publications@Marquette, 2011.

[Pas19] Ralf Paschke. Hypothalamus-Hypophysen-Schilddrüsen-System. In Hans-Christian Pape, Armin Kurtz, and Stefan Silbernagl, editors, *Physiologie*. Georg Thieme Verlag KG, 9th edition, 2019.

[PMB14] B. Pandiyan, S. J. Merrill, and S. Benvenga. A patient-specific model of the negative-feedback control of the hypothalamus-pituitary-thyroid (hpt) axis in autoimmune (hashimoto's) thyroiditis. *Mathematical Medicine and Biology*, 31(3):226–258, September 2014.

[Sal02] Andrea Saltelli. Sensitivity analysis for importance assessment. *Risk Analysis*, 22(3):579–590, June 2002.

[SLP+90] C. A. Spencer, J. S. Lopresti, A. Patel, R. B. Guttler, A. Eigen, D. Shen, D. Gray, and J. T. Nicoloff. Applications of a New Chemiluminometric Thyrotropin Assay to Subnormal Measurement. *The Journal of Clinical Endocrinology & Metabolism*, 70(2):453–460, February 1990.

[Sob93] I. M. Sobol'. Sensitivity estimates for nonlinear mathematical models. *Mathematical Modelling and Computational Experiments*, 1(4):407–414, 1993.

[Sob01] I.M Sobol'. Global sensitivity indices for nonlinear mathematical models and their monte carlo estimates. *Mathematics and Computers in Simulation*, 55(1-3):271–280, February 2001.

[SP97] Rainer Storn and Kenneth Price. Differential evolution – a simple and efficient heuristic for global optimization over continuous spaces. *Journal of Global Optimization*, 11(4):341–359, 1997.

[TCC20] Michel Tosin, Adriano M. A. Côrtes, and Americo Cunha. *A Tutorial on Sobol' Global Sensitivity Analysis Applied to Biological Models*, volume 32, pages 93–118. Springer International Publishing, 2020.

[YRFSD14] Ruoting Yang, Maria Rodriguez-Fernandez, Peter C. St. John, and Francis J Doyle. Systems biology. In Ewart Carson and Claudio Cobelli, editors, *Modelling Methodology for Physiology and Medicine*, pages 159–187. Elsevier, Oxford, 2nd edition, 2014.

[YTH+21] Boya Yang, Xi Tang, Michael J. Haller, Desmond A. Schatz, and Libin Rong. A unified mathematical model of thyroid hormone regulation and implication for personalized treatment of thyroid disorders. *Journal of Theoretical Biology*, 528:110853, 2021.